

Received 6 April 2024, accepted 28 May 2024, date of publication 6 June 2024, date of current version 25 June 2024.

Digital Object Identifier 10.1109/ACCESS.2024.3410833

RESEARCH ARTICLE

A Systematic Kidney Tumour Segmentation and Classification Framework Using Adaptive and Attentive-Based Deep Learning Networks With Improved Crayfish Optimization Algorithm

VINITKUMAR VASANTBHAI PATEL¹, ARVIND R. YADAV², PRATEEK JAIN², (Member, IEEE),
AND LINGA REDDY CENKERAMADDI³, (Senior Member, IEEE)

¹Electronics and Communication Engineering Department, Parul Institute of Engineering and Technology, Parul University, Vadodara 391760, India

²Electronics and Instrumentation Engineering, Institute of Technology, Nirma University, Ahmedabad, Gujarat 382481, India

³Department of Information and Communication Technology, University of Agder, 4879 Grimstad, Norway

Corresponding author: Linga Reddy Cenkeramaddi (linga.cenkeramaddi@uia.no)

ABSTRACT Kidney illness constitutes a category of many serious persistent diseases that can affect an individual. Early diagnosis of this condition is critical for effective therapy. Kidney tumours are the 2nd most common type of urological tumour. They come in a variety of forms, the majority of which are cancerous. In comparison to the laborious and lengthy conventional evaluation, deep learning's autonomous detection techniques may reduce diagnostic time, enhance the precision of tests, lower expenses, and minimize the radiologist's burden. It is difficult for clinicians to distinguish kidney cancers from renal Computerized Tomography (CT) images. During an operation, the precise division of kidney tumours can assist physicians in determining tumour intricacy and severity. However, due to their variety, segmenting renal tumours mechanically might be challenging. Therefore, an intellectual kidney tumour segmentation and classification model is implemented to recognize benign and malignant tumours at an early stage. To execute this procedure, the input CT images are gathered from standard websites. Then these images are given to the proposed 3D-Trans-Residual DenseUnet++ (3D-TR-DUnet++) network for the segmentation process. With the help of the segmentation process, doctors can identify the normal and abnormal regions in the kidney. The segmented images are then preceded by the classification stage. To classify kidney tumours, a deep learning-based method called Adaptive and Attentive Residual Densenet with Gated Recurrent Unit (AA-RD-GRU) is developed. Here, the parameters from this network are optimized via the recommended Modified Crayfish Optimization Algorithm (MCOA). The precise segmentation and classification of tumours in the kidney help to provide better treatments at the correct time. The segmentation and classification results are contrasted with other deep learning networks as well as various optimization algorithms.

INDEX TERMS Kidney tumour segmentation and classification, deep learning-based image analysis, 3D-Trans-Residual DenseUnet++, adaptive and attentive based residual DenseNet with gated recurrent unit, modified crayfish optimization algorithm.

The associate editor coordinating the review of this manuscript and approving it for publication was Roberta Palmeri¹.

I. INTRODUCTION

Kidneys are essential glands in the body's urinary tract because they excrete toxins from the circulatory system,

regulate the equilibrium among body electrolytes and fluids, regulate blood sugar levels, and participate in the production of hormones [1]. It maintains the human body's water and electrolyte equilibrium by releasing and purifying waste. It additionally secretes a variety of proteins and aids in controlling high blood pressure. Cancer of the kidneys ranks as one of the most prevalent ten cancers in both men and women. The chance of developing cancer in the kidneys is approximately 1 in every 75 (1.34%). Renal carcinoma (RC) is a life-threatening urological illness affecting approximately 400,000 people each year [2]. Kidney illnesses are a major public health concern around the world. In 2018, 175,000 people died of cancer of the kidneys, accounting for around 1.8% of total cancer fatalities worldwide [3]. Techniques for evaluating kidney health are likely to help with the progression of the disease, estimation, diagnosis, therapy, and possibly early detection of kidney abnormalities. CT produces high-resolution pictures with significant anatomic information [4]. As a result, it is important to determine the extent of kidney problems. Kidney segments in CT scans can help surgeons schedule surgeries; calculate total renal size to predict renal function, and aid clinical physicists or specialists with disease diagnosis and development [5]. Renal cell carcinoma (RCC) represents the third highest illness incidence, first and second are prostate cancer and bladder cancer. With newly identified 48,780 cases and 27,300 annual occasions for RCC-related mortality in the US alone, RCC is considered to be the seventh-most prevalent cancer among men and the ninth-highest frequent disease in women [6]. On imaging, identifying benign kidney cancers from aggressive carcinomas of renal cells might be difficult. However, nearly all of the renal tumours are malignant. The overwhelming majority of these kinds of tumours are RCC [7]. The most frequent type of kidney RCC is distinct cellular RCC, which accounts for roughly 80-90% of the total kidney malignancies. Over the past twenty years, the global prevalence has climbed by 2% every year. Kidney tumours have grown more prevalent, and the illness can progress for years without signs [8]. Over 50% of the instances of carcinoma of renal cells may have been detected by chance. Additionally, no underlying cause of cancer of the kidneys has yet been identified. Tobacco use, being overweight, inadequate nutrition, significant consumption of alcohol, relatives with a heritage of high blood pressure, being around irradiation and chlorine substances, and genetics are all causes of sickness [9]. The role of a healthy kidney along with kidney tumour symptoms and diagnosis is represented in Fig. 1.

II. WHY KIDNEY TUMOR SEGMENTATION AND CLASSIFICATION FRAMEWORK IS REQUIRED?

The manual renal division is a laborious and time-consuming task that might produce inconsistencies. Radiologists must devote an enormous amount of energy to analyzing the large number of CT scans [10]. Their expertise has a big

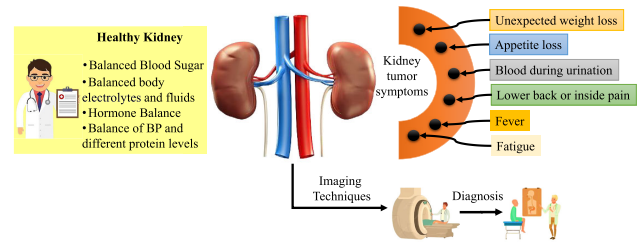


FIGURE 1. The role of a healthy kidney along with present tumour symptoms and diagnosis.

impact on the effectiveness of segmentation. Furthermore, human eyes may be unable to appropriately segment some hazy regions. The careful labeling of numerous CT scans is quite costly [11]. To meet medical demands, a computerized kidney segmentation technique is necessary. Because of the variability in position and roughness in the form of problematic kidneys, effective segmentation of the renal area using CT scans of the gastrointestinal tract is difficult. Traditional kidney segment approaches rely heavily on computational imaging methods [12]. Setting a threshold to separate images into monochrome images is an effective approach. Manually identifying cyst sites on such scans of CT takes a significant amount of effort and time [13]. As a result, deep learning techniques for semantically segmenting have been created to find and define renal regions at the same time [12]. These approaches enable automated and exact renal and tumour segmentation, aiding disease evaluation and treatment. It may additionally enhance labor as well as the economy [14]. Lastly, the outcomes of these procedures are reliable and highly precise. The paper's organization is described below. The significance of tumour segmentation is described in section II. The prior related work is represented and the problem statement is explained in Section III. Challenges addressed and novel contributions are explored in section IV. Innovative kidney tumour segmentation and classification framework using an adaptive and attentive-based deep learning network with an improved optimization algorithm are shown in Section V. The development of a deep-learning model for kidney tumour segmentation is provided in Section VI. An adaptive and attentive-based deep learning network for the kidney tumour classification model is available in Section VII. Proposed classification methods with analysis are explored in section VIII. The result and discussion are offered in Section IX and the conclusion is accessible in Section X.

III. LITERATURE SURVEY

A. RELATED WORKS

In 2022, causey et al. introduced the Kidney Tumor Segmentation Competition (KiTS19) 2019 Arkansas AI-Campus resolution approach [15]. A synopsis of the instruction, evaluation, and verification outcomes for this significant medical image processing problem was given by the built model. After evaluating numerous model iterations, a group

of U-Net representations was created as the basis for deep learning. On both the final contest impartial test database and the neighborhood testing dataset, the algorithm consistently performed well. The model obtained kidney and carcinoma segmented Dice values of 0.949 and tumours segment Dice values of 0.601 for the initial local examination, and Dice values of 0.9470 as well as 0.6099 for the last competitive examination, correspondingly. In 2021, Hussain et al. suggested a combined deep-learning strategy for (i) renal identification in CT images and (ii) segmentation-free kidney size estimate in CT scans [16]. A selection-convolutional Neural Network (CNN) was employed in the localized approach to calculate the kidney's inferior-superior spanning in the direction of axial rotation. The calculated span's longitudinal slicing was then employed in an integrated longitudinal-axial Mask Region-Based CNN (Mask-RCNN) that accepted the organ's boundaries based on the axis and longitudinal slices, resulting in an ultimate 3D organ boundary box. In addition, a network of convolutions was employed to calculate kidney quantity, bypassing the division phase. An equation was also developed to approximate the 'weight inaccuracy' metrics derived from the 'Sensen-Dice factor.' To verify the approach, 100 individuals' CT scans were taken using Vancouver General Hospital's documents, and 210 individuals' CT images were retrieved through the 2019 Renal Tumor Segment Challenge databases. The approach had a 2.4mm renal barrier error in localization and a 5% average capacity estimate error. In 2022, Hasiao suggested kidney segmentation using an encoder-decoder design [17]. A process of parameter optimization was put into place, which involved building a mathematical structure, choosing a loss rate and windows technique, and augmenting the information. Using a Dice value of 0.969 based on the 2019 Renal and Organ Tumour Segmentation Challenge database, the algorithm featuring an encoding of EfficientNet-B5 with a decoding component of a characteristic pyramid structure produced the best results. The kidneys and cancer sizes, histological planes, and voxel gaps of the suggested model were varied during testing. In addition, segmentation anomalies were examined through instances. Lastly, the generated model was assessed using a five-fold cross-validation approach and the 3D-IRCAD-01 database about the assessment criteria of the Dice rating, recall, accuracy, and the intersection over Union (IoU) rating. Overall, the trial findings demonstrated the potential practical applications of the suggested kidney segmentation algorithms in CT scans to support physicians during preparation for surgery. In 2023, Pavarut et al. created a powerful model that works better than the current approach of employing single-modal healthcare pictures to enhance the results of classification [18]. To do this, the abundance of multidimensional information obtained from Magnetic Resonance Imaging (MRI) and Contrast-Enhanced CT (CECT), as well as their corresponding subgroups, was used to identify which particular modalities or pair best

aids in categorization. The paper established an in-depth analysis of the various multi-modal fusing strategies, using the Area under the Curve (AUC) as the standard for assessing efficiency. Furthermore, this work addressed the issue of kidney tumour data not being easily accessible by employing Conditional CycleGAN, a component of translated images that translates across two distinct picture areas, to recover a portion using the existing data. By using multi-modal fusing methods and the suggested method for recovering missed data, the study has produced better classification outcomes than single-modal categorization methods. In 2019, Yu et al. introduced Crossbar-Net, a cascaded adaptable segmented network [19]. The technique blended two cutting-edge plans: 1) The upward patching and the plane patching, two perpendicular non-squared areas, were suggested as the border patches. The kidney cancers' global and local appearances might be concurrently recorded by the crossbar sections in both horizontal and vertical planes. 2) The two sub-models (the vertical as well as horizontal parts) were repeatedly learned in a transmitted learning manner using the generated crossbar patchwork. The trained separate models were urged to grow centered on the challenging areas of cancer during learning (i.e., mis-segmented areas). To be more precise, the sideways (vertical) sub-model needed the assistance of the vertically horizontally sub-model in order to divide the incorrectly divided areas. As a result, before convergence, both sub-models might function in concert to enhance themselves. In the study, the approach was assessed on a genuine database of CT kidney cancers; comprising 3500 CTs, gathered from 94 distinct individuals. The findings showed that the method performed better on the Dice similarity factor, real-positive fraction, centroid geographical separation, and Hausdorff distance tests compared to the cutting-edge segmentation techniques. In 2021, [5] suggested using CNN for the segmentation and categorization of kidney cancers to increase the precision of kidney tumour segment and categorization and to aid medical professionals in the detection. Kidney tumour classification and segmentation were combined to create the assignment using the Two-Task Neural Network (2D-SCNet). According to the suggested structure, segmentation might assist the system in concentrating on specific characteristics and areas of interest (ROI), while categorization might offer input on the net's overall knowledge of the environment. Each job increases previous knowledge of one another and works together to boost system learning. When the classification and segmentation of 2D-SCNet were combined, the correctness rate for both benign and cancerous classifications could exceed 99.5%. The cross-validation findings demonstrated that kidney tumour classification and segmentation activities might be performed effectively by the 2D-SCNet technique. In 2020, [20] Several cutting-edge neural network algorithms have been developed to identify kidney or carcinoma regions in CT scans automatically. To increase precision, only the design of the neural network

changed in the majority of these models. Preparing the data, nevertheless, proved to be an essential step in enhancing the outcomes. The pre-processing techniques that must be used before analyzing medical pictures in a model based on neural networks were methodically covered in this paper. According to the results of the study, the suggested methods for pre-processing or algorithms considerably increase the precision rate when compared to the scenario in which data preliminary processing was not done. The suggested medical imaging processing techniques as well as deep models for learning made efficiency appropriate for clinical tasks requiring less computing power. Accurate tumour identification and automated kidney capacity computation were accomplished with cost-effectiveness and efficiency. In 2020, Ruan et al. created a Multi-Branch Featured Sharing Generating Adversarial Network (MB-FSGAN) to quantify and classify renal cancers on CT at the same time [21]. The components of MB-FSGAN were the Features Sharing Generating Adversarial Network (FSGAN), Location of The Region of Interest (LROI), and multiple scales feature extractor (MSFE). Strong semantic data was produced by MSFE on feature graphs of various scales, and this is very useful for identifying tiny tumour targets. The tumour's area significance was retrieved by the LROI, significantly lowering the system's temporal cost. Through combined instruction and adversarial acquiring knowledge, FSGAN efficiently exploited the parallels and contrasts among the two linked tasks, appropriately segmenting and quantifying kidney cancers. The outcomes demonstrated the network's dependable operation, efficacy, and promise as a therapeutic tool.

B. PROBLEM STATEMENTS OF PRIOR WORKS

Kidney tumour classification is a vital component of diagnostic imaging and treatment. Conventional kidney tumour segmentation and classification models face more challenges. Table 1 explores the features and challenges of the conventional kidney tumour segmentation and classification models. Ensemble of U-Net [15] computing cost of this method is less and the outcomes are more accurate and comparable to ground true photographs. However, this approach makes extensive use of volumetric variables. Cascaded Regression Neural Nets [16] effectively recognizes and diagnoses the dimension and position of malignant cells and performs accurate quantifying and segmentation on renal cancers. However, this system is inconsistent during development and processes at a more gradual pace. Encoder-decoder [20] can catch components flowing at a quicker frequency despite tiny kernels. However, this architecture necessitates a greater memory need and processing expense. Conditional CycleGAN [18] produces high-accuracy segmented data and proves more resilient. However, the occurrence of renal hollows, artery walls, and venous complicates segmentation. Crossbar-Net [19] quickly extracts important properties of various magnitudes and dimensions. But it has a reduced

memory. As a result, it fails to grow effectively on larger systems. 2D-SCNet [5] requires less computing time and resources to be trained, but this technique is not appropriate for bad-quality CT scans or inaccurate information. CNN [20] process is easy, has a higher reproducibility, and yields the amount of fluid from a renal in an organized and affordable manner. However, it is only intended for the identification of renal lesions using CT images. As a result, it's unable to effectively partition various organs with separate modalities. MB-FSGAN [21] improves the field of receptivity. But the whole process is delayed. So, we designed a novel kidney tumour segmentation and classification model to alleviate the issues.

IV. NOVEL FRAMEWORK OF IMAGE SEGMENTATION AND CLASSIFICATION TO THE STATE OF THE ART FOR KIDNEY TUMOR DETECTION

A. RESEARCH QUESTION AND CHALLENGES ADDRESSED IN THE CURRENT PAPER

Kidney feature extraction using CT scans often relies on strong shifts in intensity between voxels that surround the kidney margin [22]. Nevertheless, when obtaining CT images, multiple issues like poor contrast, sound, opaqueness, and anisotropic may occur. If uncertain voxels emerge around unit borders, segmentation outcomes will be affected. The attributes obtained do not entirely represent the contour of the kidneys. Furthermore, the efficiency of malignancies and the textural similarity between tumours and kidneys might make diagnosis difficult. As a consequence, practical tasks continue to be difficult [23]. To address these issues, conceptual segmentation techniques based on Convolutional Neural Networks (CNNs) have been developed. Modified CNNs can require more data for training to conduct precise segmentation eliminating the need for human interaction. The preparation of data is critical in the procedure of segmentation to create better-trained algorithms [24].

B. NOVEL CONTRIBUTION OF THE PAPER

Improved and cleaned data, together with the ground truth and training database can increase segmentation accuracy in some applications related to medicine. So, an effective kidney tumour segmentation model has been developed to alleviate such challenges, and its contributions are given as follows:

- Proposed Design of the kidney tumour segmentation and classification model using a deep learning strategy aids in accurately identifying, treating, and evaluating kidney tumours.
- Judiciary claimed more specific assessments of tumours, the effective 3D-TR-DUnet++-based kidney tumour segmentation model is developed by comprising the DenseUnet++ with transformer network for accurately segmenting the affected area to make the classification process easier. Additionally, this process increases the quality of the image and also minimizes the processing time.

TABLE 1. Features and challenges of conventional kidney tumour segmentation and classification models.

Author [citation]	Methodology	Features	Challenges
Causey et al. [1]	Ensemble of U-Net	- The computing cost of this method is less. - The outcomes have greater accuracy and are comparable to ground true photographs.	- This approach makes extensive use of volumetric variables.
Hussain et al. [2]	Cascaded Regression Neural Nets	- It effectively recognizes and diagnoses the dimension and position of malignant cells. - It performs accurate quantifying and segmentation on renal cancers.	- This system is inconsistent during development and processes at a more gradual pace.
Hsiao et al. [3]	Encoder-decoder	- This approach can catch components flowing at a quicker frequency despite tiny kernels.	- This architecture necessitates a greater memory need and processing expense.
Pavarut et al. [4]	Conditional CycleGAN	- It produces high-accuracy segmented data. - This approach proves more resilient.	- The occurrence of renal hollows, artery walls, and venous complicates segmentation.
Yu et al. [5]	Crossbar-Net	- This approach quickly extracts important properties of various magnitudes and dimensions.	- It has a reduced memory. As a result, it fails to grow effectively on larger systems.
Gong and Kan [6]	2D-SCNet	- It requires less computing time and resources to be trained.	- The technique is not appropriate for bad-quality CT scans or inaccurate information.
Hsiao et al. [7]	CNN	- This process is easy and has a higher reproducibility. - This method yields the amount of fluid from a renal in an organized and affordable manner.	- This approach is only intended for the identification of renal lesions using CT images. As a result, it's unable to effectively partition various organs with separate modalities.
Ruan et al. [8]	MB-FSGAN	- This approach improves the field of receptivity.	- The whole process is delayed.

- To correctly detect and classify various forms of kidney tumour, a novel AA-RD-GRU-based kidney tumour classification system is designed by embedding the residual DenseNet with GRU. This helps to increase the survival of the patients through early identification, making use of parameter optimization. In addition, this suggested AA-RD-GRU networks help to minimize the error rates of the process.
- To enhance the accuracy, the MCOA algorithm is implemented by modifying the conventional Crayfish Optimization Algorithm (COA) for tuning parameters like hidden neurons, number of epochs, and step per epoch in the AA-RD-GRU-based kidney tumour classification system.
- To confirm the usefulness of the designed model, the performance is compared and explored with various state-of-the-art schemes based on segmentation and classification performance on kidney tumours and proved its superiority.

V. AN INNOVATIVE KIDNEY TUMOR SEGMENTATION AND CLASSIFICATION FRAMEWORK USING ADAPTIVE AND ATTENTIVE-BASED DEEP LEARNING NETWORK

A. IMPLEMENTED KIDNEY TUMOR SEGMENTATION AND CLASSIFICATION FRAMEWORK

Kidney tumour classification is a vital component of diagnostic imaging and treatment. It involves evaluating clinical images, including CT images, to identify the kinds and features of kidney cancers. Yet, this effort presents

a unique variety of obstacles. A problem is the variation in cancer appearances. Kidney tumors may differ in size, form, and appearance, rendering it hard to create a universal categorization model. Tumors may possess traits with non-tumor entities, confounding the categorization procedure. Another problem is the high incidence of uncommon or unusual tumor subgroups. While many kidney tumors can be classified into basic kinds, there are a few cases wherein tumors have distinct traits that cannot be categorized easily into established classification methods. Identifying and correctly distinguishing these unusual variants can be difficult, and specialized knowledge and an in-depth comprehension of tumor biology are needed. Furthermore, the accessibility of the information labeled for training is a barrier. Accurate models of classification require a big database of labeled images. Yet, collecting enough labeled information for kidney tumor classification may prove laborious and costly. Limited availability of labeled data can impede the creation and evaluation of effective classification systems. In addition, verifying the ability to be generalized and the consistency of categorization models is essential. Various imaging modalities, collection techniques, and resolution variations all have a bearing on the classification efficiency of algorithms. It is critical to create systems that accurately identify kidney tumours across multiple diagnostic systems and scenarios. In summary, kidney tumor classification confronts obstacles such as tumor variation, rare variants, labeled availability of data, generalization, and the incorporation of new technology. To address these problems, healthcare providers, investigators, and technologies will need to work together

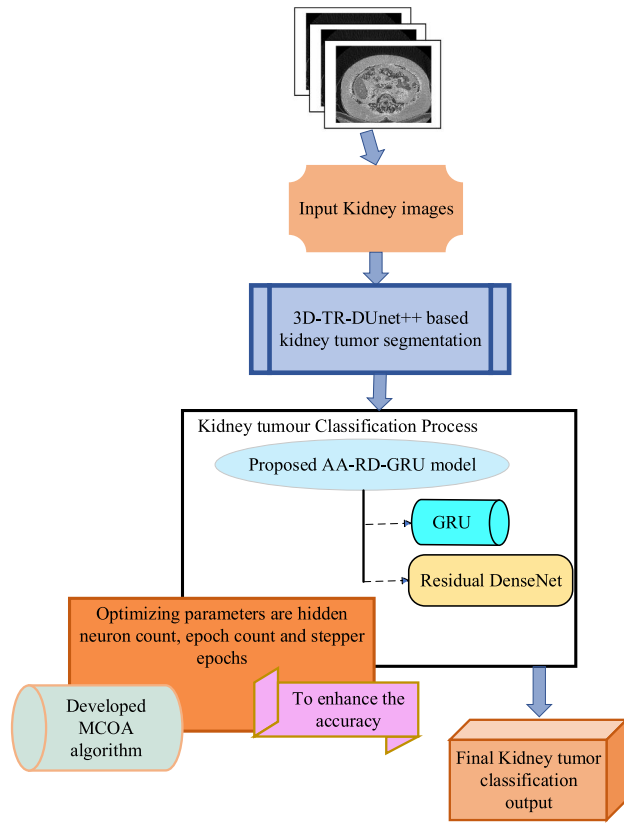


FIGURE 2. Schematic illustration of the proposed kidney tumour segmentation and classification system.

to create solid and trustworthy classification algorithms that can help in the precise assessment and planning of therapy for renal carcinoma sufferers. As a result, an intellectual kidney tumour segmentation and classification system is employed to identify benign and malignant tumours at their earliest stages. Fig. 2 displays a schematic illustration of the proposed kidney tumour segmentation and classification system. The designed deep learning-assisted kidney tumour segmentation and classification system is used for effectively classifying the kidney tumour through the segmentation process. The proposed model provides reliable tumour classification outcomes and thus helps in choosing patients for clinical testing, resulting in effective kidney malignancies. Initially, the input CT images originated from regular websites. The images are subsequently entered into the established 3D-TR-DUnet++ system for segmentation. The segmentation procedure allowed clinicians to detect normal and pathological sections in the kidney. The segmented images then proceed to the classification phase. To classify kidney tumours, a deep learning-based technique AA-RD-GRU is developed. The parameters in the developed AA-RD-GRU system like hidden neurons, epochs, and step per epoch are optimized using the suggested MCOA to enhance the accuracy. The exact segmentation and classification of kidney tumours assist in getting rid of more effective medicines

at the appropriate time. The segmentation and classification outcomes are compared with different deep learning networks and optimized functioning strategies.

B. KIDNEY TUMOR CT IMAGE DATASET

The images needed for performing the developed model are shown as follows. The images are taken from Kits19-2 dataset. This database contains 2 specific files, (i) imaging (985.66 MB) and (ii) segmentation (123.21 MB). The size of the file is 53.76 GB. The images are garnered via Dataset-2 (“KiTS21 database”). This file has code employed for processing and importing information from the system. The collected images are provided in Table 2 and indicated by the term KiT_T^{Gar} .

C. PARAMETER OPTIMIZATION SUPPORTED BY INTRODUCED MCOA

The MCOA algorithm is designed to enhance the performance of the developed kidney tumour segmentation and classification model through optimization. The MCOA is developed based on the conventional COA. The COA is notable for its effectiveness in resolving complicated optimization issues by emulating crayfish behavior in their native environment, as well as its capacity to seek worldwide optimal, which implies it can discover the optimal answer out of all conceivable options. It is resilient and capable of solving optimization issues with many different factors, restrictions, and targets. However, it may take a considerable number of repetitions to reach an ideal solution, particularly for complicated issues. This will result in longer calculation instances, and efficiency might be susceptible to starting conditions, implying that various starting points may produce outcomes that vary. For such pros and cons, we introduced a modified form of COA named MCOA; this tunes the parameters like hidden neurons, epochs, and step per epochs in the developed AA-RD-GRU model for increasing accuracy. Eq. 1 aids in updating the random value using the adaptive concept.


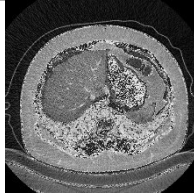

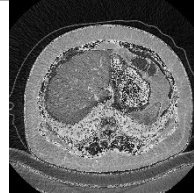

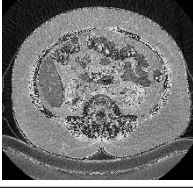
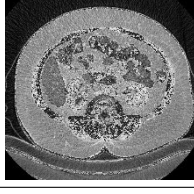
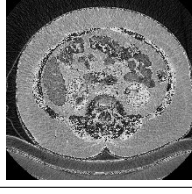
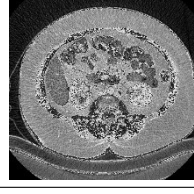
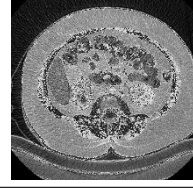
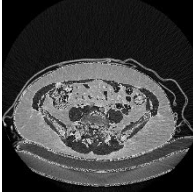
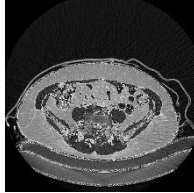
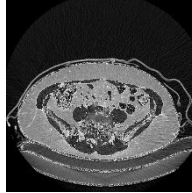
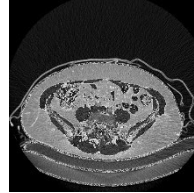
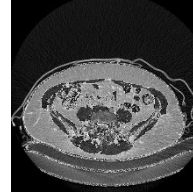
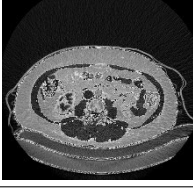
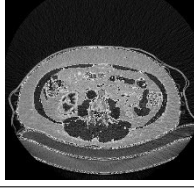
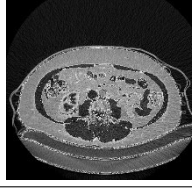
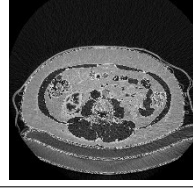

$$Rnd = \frac{ET}{\left(\frac{OT}{AT}\right)} \quad (1)$$

Here, the terms ET , AT , and OT define the bestfit, worstfit, and meanfit respectively.

D. CRAYFISH OPTIMIZATION ALGORITHM (COA)

Crayfish scavenging vacation time, and aggressive behavior influenced COA [25]. The exploiting phase of COA constitutes the hunting phase, while the searching stage is the peak summer vacation phase. The crawfish colonies are defined at the beginning of the procedure to reflect the properties of swarm-based optimization. The term B_m corresponds to the n^{th} crayfish’s status, suggesting the solution. Here, $(B_m = \{B_{m,1}, B_{m,2}, \dots, B_{m,D_m}\})$ serves as the optimization problem’s distinctive number, referred to as dimensionality). The term B_m uses a function called $j(\cdot)$ to find a solution that’s frequently referred to as the value of

TABLE 2. Collected sample CT images.

Image Description	Image-1	Image-2	Image-3	Image-4	Image-5
Kits19-2 dataset					
Normal images					
Abnormal images					
KiTS21 database					
Normal images					
Abnormal images					

fitness. The temperature, which is a randomized parameter that indicates the outside temperature of the habitat where the person is placed, governs COA exploitation and exploration. COA will proceed to the summertime vacation phase or competitive stage if its humidity rises excessively. Modify the updated solution throughout the summertime vacation phase based on the person's location B_m and the cavern location B_{Shd} . COA will move into the hunting phase once the humidity is adequate. The placement of a meal is the perfect spot, referred to as the best option, during the hunting phase. The present solution $FtNs_m$ (the solution produced by B_m) and the optimum solution $FtNs_{FuD}$ (the solution acquired by the optimum solution) are used to calculate the dimensions of the meal. Whenever food consumed is appropriate, the crayfish receive novel strategies based on their location B_m , dietary continuous t , and feed location B_{FuD} updates. Whenever the meal becomes huge, the crayfish will tear things apart with its clawed leg before eating with both of its other moving feet alternatively. Then the cosine and sine equations are utilized to recreate crayfish alternate eating habits. Crayfish regulate their food intake. Heat influences the consumption of food, which has an advantageous dispersion.

E. START THE POPULATION

Each crayfish within a multimodal optimization issue has a $1 \times D_m$ vector. Every row in the matrix indicates an issue that needs a solution. Every value B_m in an array of numbers ($B_{m,1}, B_{m,2}, ..B_{m,Dm}$) has to fall within the top and bottom bounds. COA is initialized by randomly generating a set of potential solutions B within the available space. The number of people R and dimensions D_m are used to choose a potential solution B . Eq. 2 depicts the setup of the COA method.

$$B = [B_1, B_2, ..B_R] = \begin{bmatrix} B_{1,1} & \cdots & B_{1,n} & \cdots & B_{1,Dm} \\ \vdots & \cdots & \vdots & \cdots & \vdots \\ B_{m,1} & \cdots & B_{m,n} & \cdots & B_{m,Dm} \\ \vdots & \cdots & \vdots & \cdots & \vdots \\ B_{R,1} & \cdots & B_{R,n} & \cdots & B_{R,Dm} \end{bmatrix} \quad (2)$$

Here, the term B represents the starting population status, R represents the assortment of people, D_m represents the population scale, $B_{m,n}$ represents the location of each person m in the n^{th} scale and $B_{m,n}$ value is calculated using Eq. 3.

$$B_{m,n} = pf_n + (yf_n - pf_n) \times Rnd \quad (3)$$

Here, the term pf_n signifies the n^{th} dimension's bottom bound yf_n is the n^{th} dimension's top bound, and Rnd is an

arbitrary number. This Rnd gets updated using the adaptive concept in Eq. 1.

F. TEMPERATURE AND INTAKE OF CRAYFISH

Temperature changes influence crayfish movement and cause them to progress through several phases. Eq. 4 defines temperature. Whenever a temperature rises above 30°C, the crayfish will look for a cool location to spend summertime. Crayfish will engage in foraging behavior at the optimum temp. Temperature influences how much crayfish feed. Crayfish feed well at temperatures around 15 and 30 degrees Celsius. As a result, the daily consumption quantity of crayfish may be estimated to the typical distribution, and the nutrition dose is temperature dependent. Since crayfish have a significant foraging tendency around 20 and 30 degrees Celsius. As a result, COA defines a temperature range of 20 to 35°C. Eq. 5 depicts a mathematical representation of crayfish intake.

$$T_p = Rnd \times 15 + 20 \tag{4}$$

Here, the term T_p is a measure of the surroundings in which the crayfish is found.

$$t = G_1 \times \left(\frac{1}{\sqrt{2 \times \pi \times \sigma}} \times \exp\left(-\frac{(T_p - \mu)^2}{2\sigma^2}\right) \right) \tag{5}$$

Between them, μ relates to the optimal temperature for crayfish, while the term σ and G_1 are used to regulate crayfish consumption at various degrees.

G. SUMMER RESORT PHASE

When a certain temperature exceeds 30, the heat is excessive. At this point, the crayfish will decide to spend the warmer months in the cavern. The B_{Sde} cavern is defined in the Eq. 6.

$$B_{Sde} = \frac{(B_K + B_P)}{2} \tag{6}$$

Here, the term B_K indicates the best position gained at this point by the number of repetitions, and B_P reflects the best spot in the present population. Crayfish fighting for tunnels happens randomly. If $Rnd < 0.5$, there are no additional crawfish fighting for caverns, and the crawfish will head into the cave straight for their summer break. Applying Eq. 7, the crayfish will make its way into the cavern for their summer vacation around that point.

$$B_{m,n}^{x+1} = B_{m,n}^x + G_2 \times Rnd (B_{Sde} - B_{m,n}^x) \tag{7}$$

Here, the term G_2 indicates a declining curve, as stated in Eq. 8, where x denotes the latest iteration frequency and $x + 1$ indicates the following generation repetition count. The term Rnd is the random value this can be amended using the adaptive concept in Eq. 1.

$$G_2 = 2 - \left(\frac{x}{X}\right) \tag{8}$$

Here, the term X denotes the largest number of repetitions. Crayfish's objective in the summertime resort level is to reach

the cellar, so this is the best option. The crayfish will be approaching the cavern at this juncture. This puts folks nearer to the best option and improves COA's exploit capability. Allow the method to come together more quickly.

H. STAGE OF COMPETITION (EXPLOITATION)

When $T_p > 30$ and the $Rnd > 30$, it indicates that other crayfish are additionally keen on the cave. They are battling for shelter at this moment. Through Eq. 9, the crayfish fights for the entrance to the cave.

$$B_{m,n}^{x+1} = B_{m,n}^x - B_{d,n}^x \times B_{Sde} \tag{9}$$

When d denotes an arbitrary crayfish person, as indicated in Eq. 10.

$$d = Round(Rnd \times (R - 1)) + 1 \tag{10}$$

Crayfish compete against themselves in the competitive phase, and crayfish modify their location according to the spot taken by another crayfish. The searching depth of COA is increased, and the algorithm's exploring capability is improved, by altering its location. Stage of foraging (exploitation): Once the temperature reaches 30, the crayfish can feed. The crayfish will begin to approach the meal at this point. The crayfish will estimate the dimensions of its nourishment after finding it. If the meal is too big, the crayfish will rip it up with its sharp claws and consume it using its second and subsequent walking foot alternatively. The term B_{Fud} is defined as an edible place in Eq. 11.

$$B_{fud} = B_K \tag{11}$$

Here, the term Fud is the food and the size of food is U , this can be defined in Eq. 12.

$$U = G_3 \times Rnd \times \left(\frac{FtNs_m}{FtNs_{Fud}} \right) \tag{12}$$

Here, the term G_3 denotes the biggest food while the constant 3, $FtNs_m$ is the fitness score of the m^{th} crayfish, and $FtNs_{Fud}$ reflects the fitness rating of the nutrient site. The crayfish's estimation of its meal size is based on the dimensions of its biggest food. When U exceeds $\frac{G_3+1}{2}$, the food being eaten is too large. The crayfish will rip off the nourishment with its first claw leg at this juncture. The following is the algebraic the following formula in Eq. 13.

$$B_{Fud} = \exp\left(-\frac{1}{U}\right) \times B_{Fud} \tag{13}$$

When the meal becomes chopped and lesser, the second and the third legs alternatively take it up as they place it in their mouths. To imitate the alternation, and manage, an amalgam of the function of sine with the function of cosine is employed. Furthermore, the nourishment obtained from crayfish is connected to the consumption of food; hence the hunting equation works using Eq. 14.

$$B_{m,n}^{x+1} = B_{m,n}^x + B_{Fud} \times t \times \left(\begin{matrix} \cos(2 \times \pi \times Rnd) \\ -\sin(2 \times \pi \times Rnd) \end{matrix} \right) \tag{14}$$

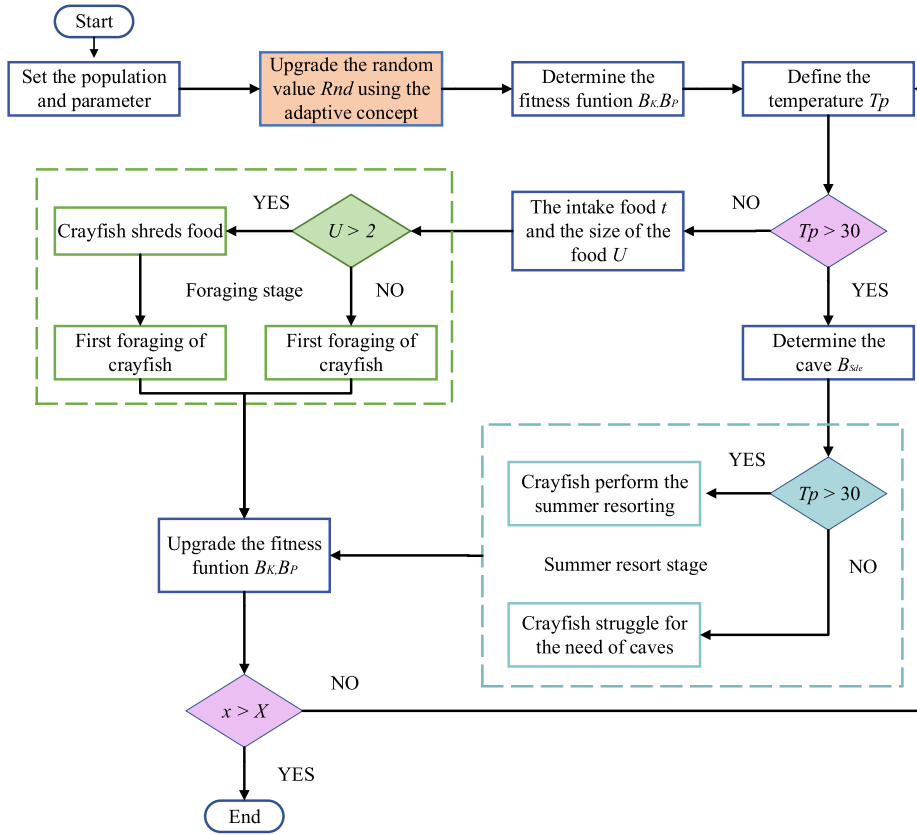


FIGURE 3. Flowchart of the proposed MCOA.

When $\frac{G_3+1}{2}$, the crayfish only needs to travel towards the meal and consume immediately, as shown in Eq. 15.

$$B_{m,n}^{x+1} = B_{m,n}^x + G_2 \times Rnd (B_{Sde} - B_{m,n}^x) \quad (15)$$

Crayfish in the Hunting phase adopt various feeding approaches according to the dimension of the food they consume U , with food B_{Fud} representing the ideal answer. When the dimension of the meal U is appropriate for crayfish consumption, the crayfish will get near its contents. When U is excessively great, it shows that the crayfish and the best solution are significantly different. As a result, B_{Fud} must have lowered and moved nearer to the meal. Adjust the unpredictability of the crayfish meal intake augmentation mechanism. The pseudo-code and the flowchart of the proposed MCOA are given in Algorithm 1 and Fig.3.

VI. DEVELOPMENT OF 3D-TRANS-RESIDUAL DENSEUNET++ FOR KIDNEY TUMOR SEGMENTATION

A. SEGMENTATION IMPORTANCE IN KIDNEY TUMOR CLASSIFICATION PERFORMANCE

Segmentation is important in kidney cancer classification because it allows for a more thorough and exact knowledge of the tumour's borders and features. Segmentation enables for more precise assessment and classification of renal tumours, leading to improved evaluation, planning of therapy, and tumour progression tracking. One of the most significant

Algorithm 1 Proposed MCOA

Initialize the iteration X , population R as well as the dimension Dm
 Generate the initialized population randomly
 Determine the population's fitness rating B_K, B_P

While $x < X$
Upgrade the random value Rnd using the adaptive concept in Eq. (1)
 Define the temperature T_p using Eq. (4)
 If $T_p > 30$
 Determine the cave B_{Sde} using Eq. (6).
 If $Rnd > 30$
 Crayfish perform the summer resorting using Eq. (7).
 else
 Crayfish struggle for the need of caves using Eq. (9)
 end
 else
 The intake food t and the size of the food U are acquired using Eq. (5) and Eq. (12)
 If $U > 2$
 Crayfish slices the food using Eq. (13)
 Foraging of crayfish using Eq. (14)
 else
 Foraging occurs using Eq. (15)
 end
 Upgrade the fitness function B_K, B_P
 $x = x + 1$
 end

advantages of segmentation in kidney tumour classification includes its capacity to properly estimate the tumour's shape

and size. This data is critical for diagnosing the tumour’s phase and extent, as well as measuring therapy efficacy. Precise volume and size data gained from segmentation enable physicians to arrive at educated choices about treatments like radiation therapy, surgery, or tailored pharmacological regimens. Segmentation additionally makes it possible for the recognition of certain tumour subdivisions or areas of concern inside a kidney tumour. By segmenting the tumour, doctors can examine distinct sections separately, providing a greater awareness of the substance and features. This knowledge can help anticipate the tumour’s behavior, determine its aggression, and provide personalized treatment strategies for patients. Furthermore, segmentation facilitates the collection of quantitative information from the tumour, such as texture, form, and brightness. These characteristics give useful data that can be employed in neural networks and forecasting algorithms to increase the precision of kidney tumour classification. By adding these traits throughout the classification management, segmentation aids in the differentiation of malignant from benign tumours, resulting in more precise classifications and improved outcomes for patients. In general, segmentation is critical in kidney tumour classification. These advantages eventually enhance kidney tumour detection, planning of therapy, and tracking, resulting in better treatment for patients and results.

B. DENSEUNET++ FRAMEWORK

The DenseUNet++ model is made by comprising the DenseNet and Unet++ [26]. DenseNet represents an indicated design of networks the fact that generated the most successful findings on various classes’ image categorization collections. Previously implemented associations, for instance, AlexNet’s neural stage, boast a high inherent dimension. The objectives of this structure would be to densely integrate various classes’ convolutional regions with exceptionally small indicative parameters. The aim of it is to join the resultant information from each of the previously convolutional layers into one with the information being provided of the following convolution circuit. Considering just q sections, $\frac{q(q+1)}{2}$ linkages could be brought in, enabling it to accommodate functions that are more complicated with fewer inputs. Dense partitioning is an assembly of this convolution, wherein the distinct magnitude of every layer is determined based on its expansion frequency. There is also the convolution layer containing a kernel based on the convolution size and width of one and a normal pooling stage combined with a kernel’s duration and breadth and step number of two among these layers.

DenseNet defines a sort of convolutional neural network. Every one of the P tiers within the system undertakes a quadratic transition K_l , if this represents the vector associated with tier p , K_p might correspond to the Batch Normalization (BN) section, Rectified Linear Units (ReLU) activation functions, and a mixture of pooling layers of convolution. The image that is input is denoted by a_0 , while the outcome of the layer p is designated by a_p .

In a typical CNN, the outcome of tier p is taken like the data source of the stage $p + 1$ and the expression is provided in Eq. (16).

$$a_p = K(a_{p-1}) \tag{16}$$

DenseNet recommends substitute connectedness architecture referred to as dense networking that will boost the transfer of knowledge across sections, through the establishment of immediate links regarding any level upward to all next ones. Layer p gets as source the attribute network for every layer before a_0, a_1, \dots, a_{p-1} and the procedure is provided in Eq. (17).

$$a_p = K_p([a_0, a_1, \dots, a_{p-1}]) \tag{17}$$

Here, the term $[a_0, a_1, \dots, a_{p-1}]$ denotes layering a function hierarchy of a_0, a_1, \dots, a_{p-1} on each channel axis.

C. PROPOSED UNET++ MODEL FOR IMAGE SEGMENTATION

UNet++ is an expansion of the UNet system that was released in the hopes of increasing the UNet design’s precision while segmenting [27]. The UNet’s encoder-decoder building keeps and claims that gradually enriching higher-resolution characteristic maps before combining them into a decoding device enables the system to gather greater excellent quality information due to greater semantic resemblance among the combined characteristics. The primary theory behind the development of the UNet++ design is the belief that by including more temporary a convolutional section and expanding the skip links among structures, the combined outcomes from every increased sampling suppression will become more similar in semantics compared to the outcomes obtained through the initial UNet construction, resulting in a simpler optimization issue resulting in more precise outcomes. The layered convolution units $A^{q,r}$ added to fill the distinction in meaning among the expanding and contracting sections of the identical layer q in the structure are linked via skipping connections having each convolutional element of the equal layer q having $p' > p$. More specifically, $A^{q,r}$ remains the results of Eq. 18.

$$A^{q,r} = \begin{cases} CB([A^{q-1,r}]) & \text{for } q = 1 \\ CB\left(\left[[A^{q-1,r}]_{n=1}^{p-1}\right], A^{q-1,r-1}\right) & \text{for } q > 1 \end{cases} \tag{18}$$

Here, the term CB is the convolution block, $CB(a)$ remains the results of the convolutional element provided as a parameter a , $[A^{l,m}]_{n=1}^i$ is the combination functioning for components $A^{l,1}, \dots, A^{l,i}$, and $[a, b]$ is the association functioning between components a and b . Fig. 4 depicts an extensive representation of the DenseUNet++ design specified within the basic UNet design.

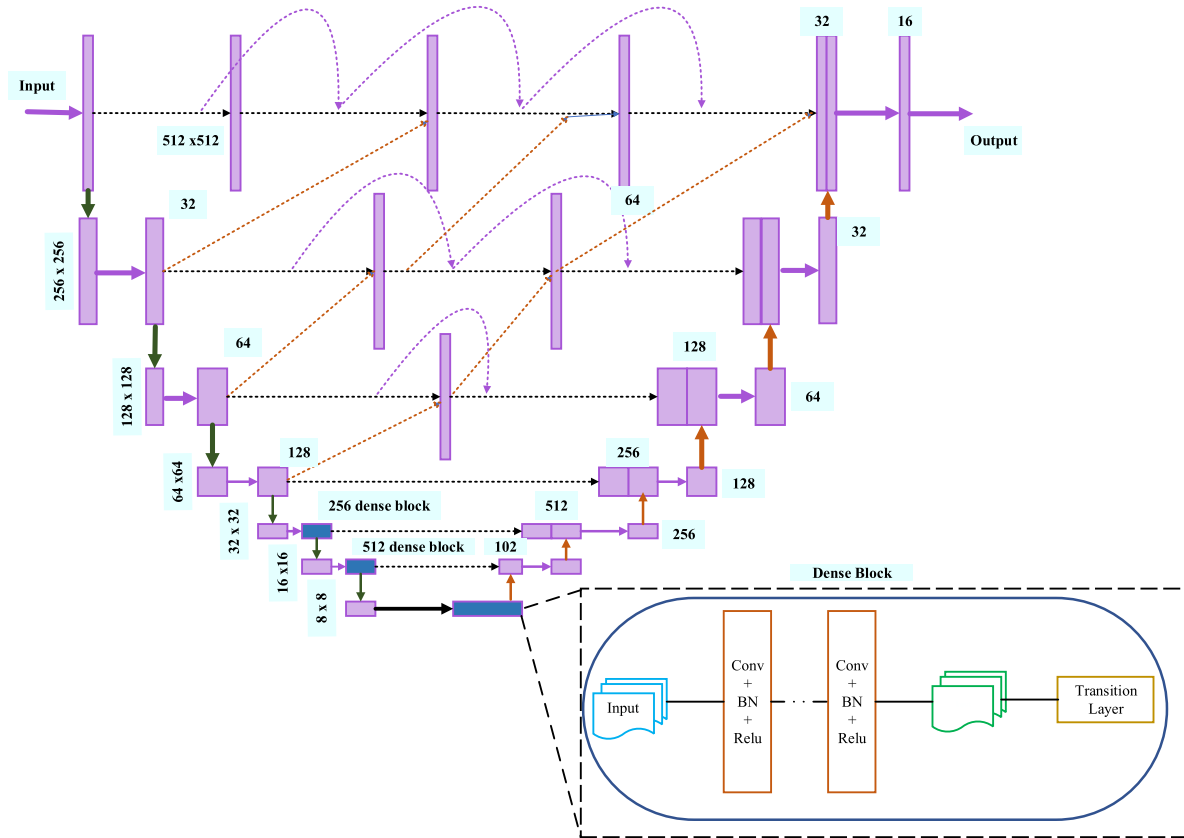


FIGURE 4. Pictorial view of the DenseNet++ model.

D. ACCURATE SEGMENTATION PERFORMANCE WITH DEVELOPED 3D-TR-DUNET++

The garnered images KiT_T^{Gar} are put as input into the designed 3D-TR-DUNet++-based kidney tumour segmentation model. This model leverages the strength of ResNet, DenseNet++, and Transformer design to produce very precise and effective results for segmentation. The transformer model receives the inputted images. The transformer model incorporates self-attention techniques, allowing the framework to detect dependence over time and improve the accuracy of segmentation. This is especially valuable in 3D healthcare imaging, wherein context is required for correct segmentation.

E. TRANSFORMER MODEL OF PRESENTED NEURAL NETWORK

The transformer circuit was built using an attention procedure, comprised of an encoding and a decoding device. The transformer system includes 8 equal layer piles, each with 2 sub-layers [28]. The multi-headed attention sub-layer includes the initial one, while the subsequent layer represents a basic fully linked forward network of neurons. A residual structure of networks connects both sub-layers, which are terminated by an average level. Here, the term $O_t = LN(a + SL(a))$, wherein every sublayer is produced

separately, expresses the final result for every sublayer, out is the output. The sub-layers within the simulation are corrected results in 256 degrees in order to simplify the residual interaction among layers. Several sublayers are explained further below.

F. DOT-PRODUCT ATTENTION FUNCTION

The attention function’s inputs T, N , and Y indicate the query, key, and value, correspondingly. The attention value is determined by the resemblance with the query key. The attention contextual is determined by the attention scales. The design employs scaling dot-product attention, determined by Eq. 19.

$$Attention(T, N, Y) = SM \left(\frac{TNW}{\sqrt{g_n}Y} \right) \tag{19}$$

G. MULTI-HEADED ATTENTION

The multi-head attention system passes T, N , and Y via k different linear changes before splicing different attention outcomes. With exact self-attention process T, N , and Y all have identical numbers as in Eq. 20.

$$MultiHead(T, N, Y) = Concatenation(H_1, H_2, ..H_k) \tag{20}$$

Here, H denotes the head. Feed-forward systems based on location. Aside from the attention sub-layer, every encoder layered includes a fully linked forward feedback circuit with a two-layer linear transform with a ReLU activating function. Then, the transformer model forwarded the processed image to the Resnet framework for further processing of the images.

H. RESNET FRAMEWORK OF PRESENTED COMPUTING MODEL

The ResNet model serves to mitigate the issue of vanishing gradients [29]. It comprises one of the frameworks created to overcome challenges in deep learning training since deep learning development requires an extended period and is restricted to a specific number of levels in general. ResNets paradigm has a benefit over other designs because its efficiency remains unchanged as the design becomes deeper. Furthermore, compute computations are thinner, and the capacity to teach networks is improved. The ResNet architecture operates by ignoring links between two and three layers of designs that feature ReLU and BN. ResNet’s residual block has been outlined using Eq. 21.

$$b = I(a, Z + a) \tag{21}$$

Here, the term a denotes the input data component, b denotes the outcome layer, and the residual mapping represents the I functional. Residual blocking on ResNet is possible when the source data sizes match the output information parameters. Furthermore, every ResNet block is made up of two or 3 layers. The first two layers of the design of ResNet are similar to GoogleNet. ResNet strengths have been set employing Stochastic Gradient Descent (SGD) with typical velocity settings. Finally, the ResNet framework passed the processed images to the DenseUnet++ model and the final segmented image outcome is obtained through this. The developed 3D-TR-DUnet model has demonstrated good performance in tumour segmentation, tissue segmentation, and defect identification. It can handle complicated and varied anatomic components, making it an important tool in healthcare image processing. The designed 3D-TR-DUnet++-based segmentation model offered the segmented image output and defined using DR_{U}^{SEG} . The graphical illustration of the segmentation performance with the developed 3D-TR-DUnet++ model is provided in Fig. 5.

VII. ADAPTIVE AND ATTENTIVE BASED RESIDUAL DENSENET WITH GATED RECURRENT UNIT FOR KIDNEY TUMOR CLASSIFICATION MODEL

A. GATED RECURRENT UNIT

GRU is a Long Short Tem Memory (LSTM)-based variation network [31]. It merges the forget gate as well as the input gate from an LSTM through an updating gate, preserving the impact generated by the LSTM but simplifying its design. As a result, the GRU exploited training as a long-term reliance characteristic. A basic GRU structure is shown in Fig. 6. The GRU needs to merely upgrade gate C_W along with reset gate U_W . The GRU persistent dependency training blocks

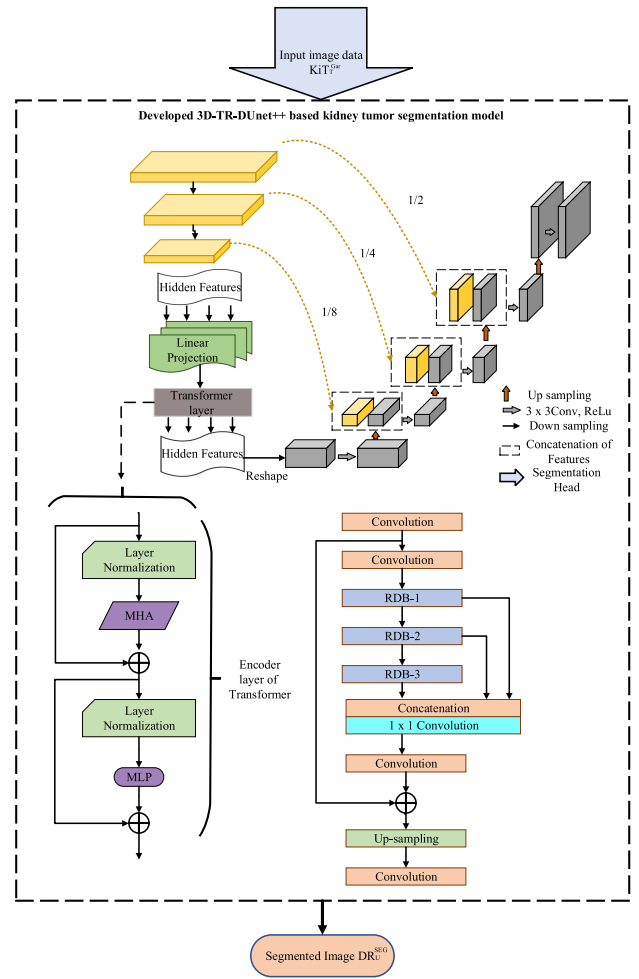


FIGURE 5. Graphical illustration of the segmentation performance with developed 3D-TR-DUnet++ model.

compute the concealed states using an array of coefficients written using Eq. 22.

$$\begin{aligned}
 C_W &= \varsigma \left(Z^{(C)} \cdot [K_{W-1}, A_W] \right) \\
 U_W &= \varsigma \left(Z^{(U)} \cdot [K_{W-1}, A_W] \right) \\
 \overline{K}_W &= \tanh \left(Z \cdot [U_W * K_{W-1}, A_W] \right) \\
 K_W &= (1 - C_W) * K_{W-1} + C_W * \overline{K}_W \tag{22}
 \end{aligned}$$

In Eq. 21, the updating gate C_W regulates how prior state data is replaced in the present state, while the resetting gate U_W regulates the degree to which past value data is discarded. The activation factor is ς . The candidate activating operation \overline{K}_W is calculated using the reset gate’s U_W (which controls the extent to which prior data is maintained) and represents the elementwise multiple operations. Lastly, K_W reflects the suggested GRU unit’s real activation at a time W that is a linear regression between the prior activation K_{W-1} with the potential activity \overline{K}_W .

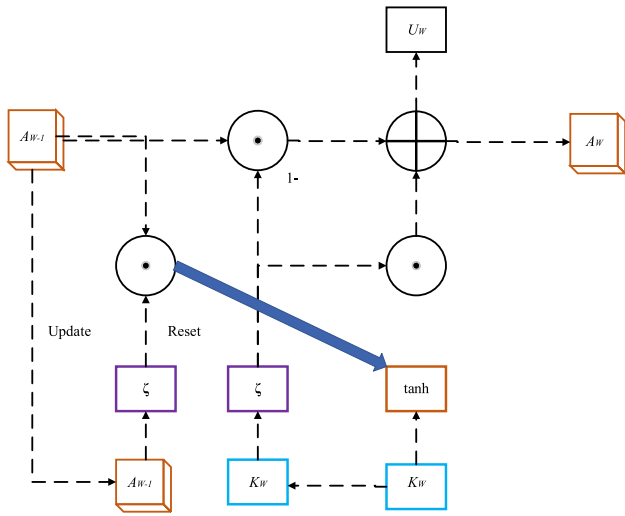


FIGURE 6. Basic structure of GRU.

B. RESIDUAL DENSENET

The Residual DenseNet [32] comprises the deep extraction of features, Residual Dense Block (RDBs), a dense fusion of features (DFF), and subsequently the up-sampling network (UPNet). Let's define L_{PT} as well as L_{KT} called RDN's inputs as well as its outputs. For the extraction of deep amenities, two convolutional layers are deployed. The term I_{-1} characteristics are taken away using the PT source from the initial convolutional module via Eq. 23.

$$I_{-1} = K_{VIH1}(L_{PT}) \quad (23)$$

Here, the term K_{VIH1} specifies the transformation method, I_1 is next used to execute incremental shallow extraction of features and residual block. As a result, Eq. 24 is obtained as an outcome.

$$I_0 = K_{VIH2}(I_{-1}) \quad (24)$$

Here, the term K_{VIH2} entails the subsequent deep extraction of features and the convolution technique that is utilized as a source of residual dense units. If there are G residual dense structures, gets the final result I_g corresponding to the g^{th} RDB using Eq. 25.

$$\begin{aligned} I_g &= K_{RDB,g}(I_{g-1}) \\ &= K_{RDB,g}(K_{RDB,g-1}(\dots(K_{RDB,1}(I_0))\dots)) \end{aligned} \quad (25)$$

Here, the term $K_{RDB,g}$ implies the g^{th} RDB's functioning, and $K_{RDB,g}$ might serve as a synthesis of procedures like compression and ReLU. While I_g is formed out of the g^{th} RDB via fully making use of every layer of convolution throughout the unit, can be considered I_g to be a local characteristic. Then dense Feature of features (DFF), following collecting complex characteristics from an assortment of RDBs. DFF takes advantage of each of the previous layers' aspects and is capable of being expressed in Eq. 26.

$$I_{DF} = K_{DFF}(I_{-1}, I_0, I_1, \dots, I_G) \quad (26)$$

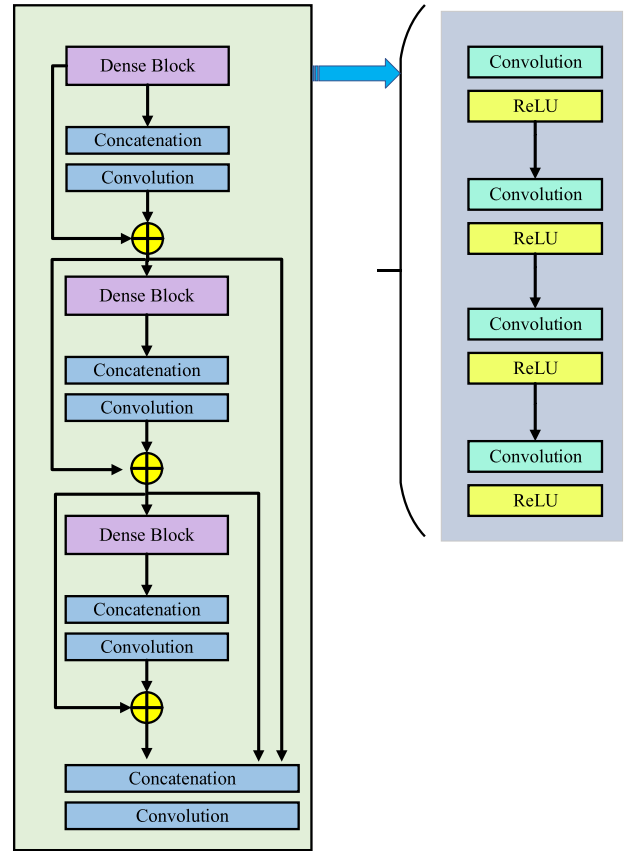


FIGURE 7. Architectural representation of the residual densenet model.

The resultant function of residual densenet is offered in Eq. 27.

$$Rs = K_{RDN}(I_{PT}) \quad (27)$$

Here, the term Rs is the resultant residual densenet. The architecture of the Residual denseNet is shown in Fig. 7.

VIII. PROPOSED AA-RD-GRU-AIDED KIDNEY TUMOR CLASSIFICATION

The segmented images DR_U^{SEG} are given as the input to the developed AA-RD-GRU-based kidney tumour classification model. Here, the developed framework combining Residual DenseNet and GRU helps to solve the problem of increasing complexity of models that can reduce additional processing time and materials for both training and inference. Furthermore, combining these two designs may increase the chance of overfitting. To overcome such drawbacks, a model should be properly tuned, so the parameters like hidden neurons, epochs, and step per epoch are optimized in the developed AA-RD-GRU model by the developed MCOA algorithm to enhance the accuracy and we introduced an attention layer within the framework to mitigate the issues mentioned above. The attention mechanism enables the framework to concentrate on important areas or characteristics in imaging tests, hence increasing the classification process's

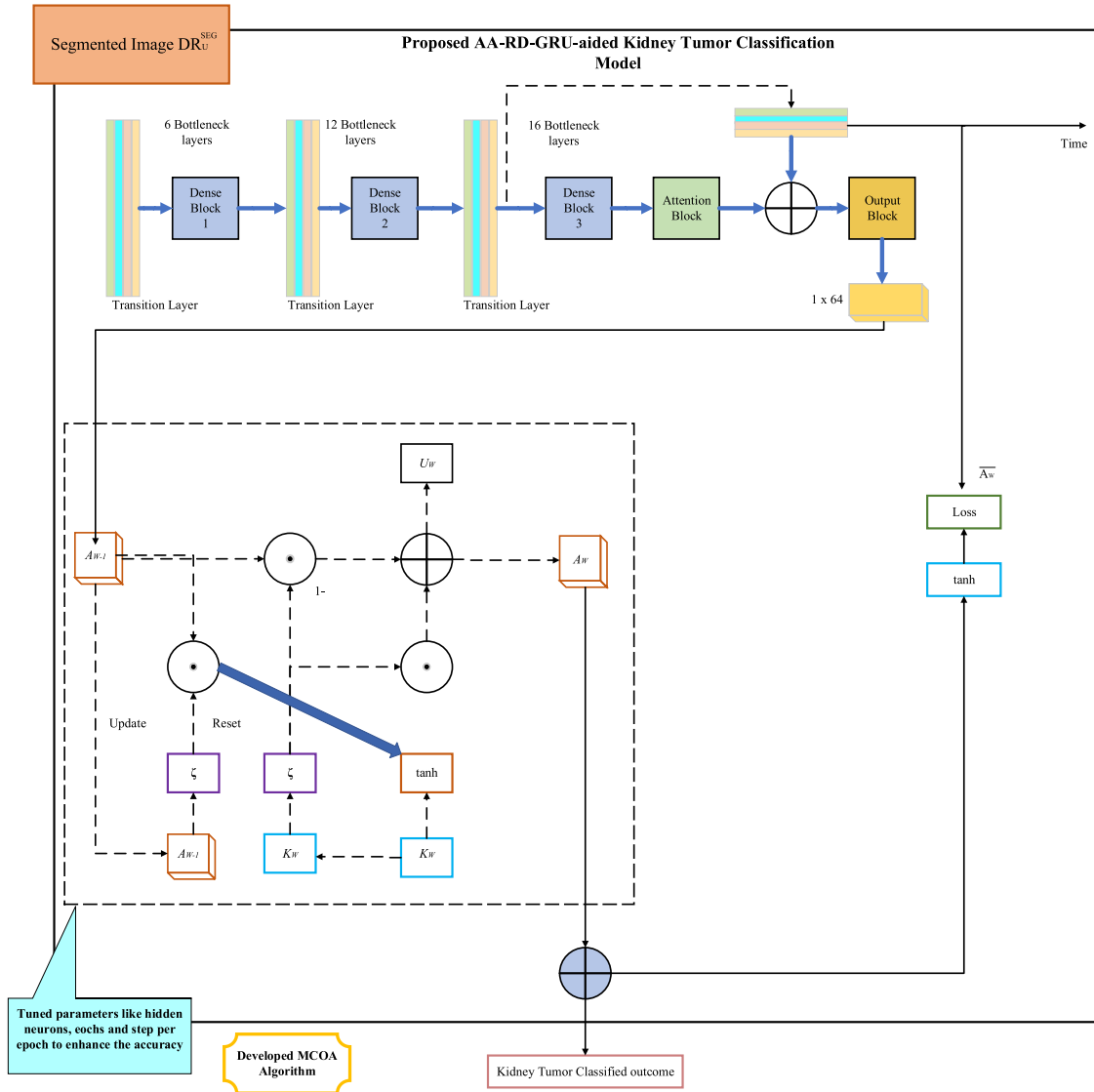


FIGURE 8. Depiction of the proposed AA-RD-GRU-aided kidney tumor classification model.

comprehension. The attention mechanism may successfully highlight significant information while suppressing unnecessary or distracting data. Finally, the developed AA-RD-GRU-based kidney tumour classification model allows for recording the spatial linkages and interconnections among various parts of the tumour, which improves classification outcomes, and then, the developed model offers the classified image outcome. Eq. 28 shows the objective function HRt_{TF} of the developed AA-RD-GRU-based kidney tumor classification model.

$$HRt_{TF} = \arg \min_{\{G_g^{ARGRU}, H_h^{ARGRU}, I_i^{ARGRU}\}} \left(\frac{1}{ArT_{RI}} \right) \quad (28)$$

Here, the term ArT_{RI} is the accuracy, and its expression is given in Eq. 29, G_g^{ARGRU} defines the hidden neurons in AA-RD-GRU in the range of [5, 255], and the terms

H_h^{ARGRU} and I_i^{ARGRU} are the epochs and step per epoch in AA-RD-GRU in the range of [5, 50] and [300, 1000].

$$ArT_{RI} = \frac{(GyB_T + FqE_C)}{(GyB_T + FqE_C + OuE_X + NsI_D)} \quad (29)$$

Here, the term pt indicates the true positive, nt defines the true negative, nf represents the false negative, and pf denotes the false positive, respectively. The diagrammatic depiction of the proposed AA-RD-GRU-aided kidney tumour classification model is illustrated in Fig. 8.

IX. RESULT AND DISCUSSION

A. EXPERIMENTAL SETUP

The developed system was executed using the Python platform and used 30 populations, 3 chromosome lengths, and a maximum iteration was 50 to complete the process.

The effectiveness of the designed framework was validated through the comparison with different existing classifiers like CNN [30], Residual Densenet [31], [32]GRU, Residual DenseNet with GRU (RD-GRU) [33], the segmentation models like UNET [34], ResUnet [35], ResUnet++ [36] and DenseUnet++ [37], and the optimization approaches like Tuna Swarm Optimization (TSO) [38], Fire Hawk Optimizer (FHO) [39], Circle Search Algorithm (CSO) [40] and COA [25].

B. PERFORMANCE MEASURES

The subsequent measures aid in evaluating the developed model.

(a) The Matthews correlation coefficient (MCC) can be done by Eq. 30.

$$CmC = \frac{GyBT \times FqEC - OuEX \times NsID}{\sqrt{\left((GyBT + OuEX)(GyBT + NsID) \right) \left(FqEC + OuEX \right) \left(FqEC + NsID \right)}} \quad (30)$$

(b) False Negative Rate (FNR) is identified via Eq. 31.

$$NeF = \frac{NsID}{NsID + GyBT} \quad (31)$$

(c) Precision Rp is obtained utilizing Eq. 32.

$$Rp = \frac{GyBT}{GyBT + OuEX} \quad (32)$$

(d) Sensitivity is resolved by Eq. 33.

$$YeS = \frac{GyBT}{GyBT + NsID} \quad (33)$$

(e) F1-Score can be recognized by Eq. 34.

$$E1S = \frac{2 * GyBT}{2 * (GyBT + OuEX + NsID)} \quad (34)$$

(f) False Positive Rate (FPR) is estimated by Eq. 35.

$$PeF = \frac{OuEX}{OuEX + FqEC} \quad (35)$$

(g) Negative Predictive Value (NPV) is classified by Eq. 36.

$$RpV = \frac{OuEX}{NsID + OuEX} \quad (36)$$

(h) Specificity is evaluated using Eq. 37.

$$YsP = \frac{FqEC}{FqEC + OuEX} \quad (37)$$

(i) False Discovery Rate (FDR) can be defined by Eq. 38.

$$BrF = \frac{OuEX}{OuEX + GyBT} \quad (38)$$

(j) The formulation of the Dice coefficient DyT can be obtained using Eq. (39).

$$DyT = 2 \times \frac{|GGs_Y^{GT} \cap DR_U^{SEG}|}{|GGs_Y^{GT}| + |DR_U^{SEG}|} \quad (39)$$

(k) The formulation of the Jaccard coefficient JyT can be obtained using Eq. (40).

$$JyT = \frac{|GGs_Y^{GT} \cap DR_U^{SEG}|}{|GGs_Y^{GT}| + |DR_U^{SEG}| - |GGs_Y^{GT} \cap DR_U^{SEG}|} \quad (40)$$

Here, the term GGs_Y^{GT} indicates the ground truth images.

C. DEVELOPED 3D-TR-DUNET++-BASED SEGMENTED IMAGES RESULTS

The developed 3D-TR-DU $net++$ -based segmented image results are provided in Table 3.

D. SEGMENTATION PERFORMANCE ON THE DESIGNED FRAMEWORK

The designed 3D-TR-DU $net++$ -based segmentation model's performance based on dataset-1 and dataset-2 are shown in Fig. 9. The proposed 3D-TR-DU $net++$ -based segmentation model given the dice coefficient value is 9.24% more than UNET, 3.65% superior to ResUnet, 4.52% enhanced than ResUnet++, and 3.44% increased than DenseUnet++ when examining the best function. The result proved that the proposed 3D-TR-DU $net++$ - segmentation framework supports accurately segmenting and diagnosing different kinds of kidney cancers and gives critical information for generating customized treatment strategies according to tumour features.

E. CONVERGENCE ANALYSIS ON THE DEVELOPED MODEL

The designed MCOA-AA-RD-GRU-based classification model's convergence performance is shown in Fig. 10. The proposed MCOA-AA-RD-GRU-based classification model offered the cost function is 52.26% more than TSO-AA-RD-GRU, 52% superior to FHO-AA-RD-GRU, 49.57% enhanced than CSO-AA-RD-GRU, and 40% increased than COA-AA-RD-GRU when 10th iteration. The result proved the proposed MCOA-AA-RD-GRU-based classification model enables individualized and focused treatment plans, resulting in excellent healthcare for patients and results. It also helps identify kidney tumours, allowing for swift action and a greater likelihood of survival.

F. DATASET-1-BASED CLASSIFICATION PERFORMANCE EVALUATION ON THE RECOMMENDED MODEL

Fig. 11 and 12 illustrate the performance results of the created MCOA-AA-RD-GRU-based classification model compared to current classifiers and optimization methodologies considering dataset 1. The proposed MCOA-AA-RD-GRU model given the accuracy is 16.35% more than CNN, 17.73% superior to Residual DenseNet, 9.88% enhanced than GRU, 1.95% increased than RD-GRU, 8.32% improved than PBS-SO-OHFD and 0.91% effective than IDF-HBA-OEC at 200th epoch. The result confirmed the suggested MCOA-AA-RD-GRU system helps physicians plan medical procedures by assuring optimal tumour eradication while maintaining normal kidney cells, as well as selecting possible scenarios

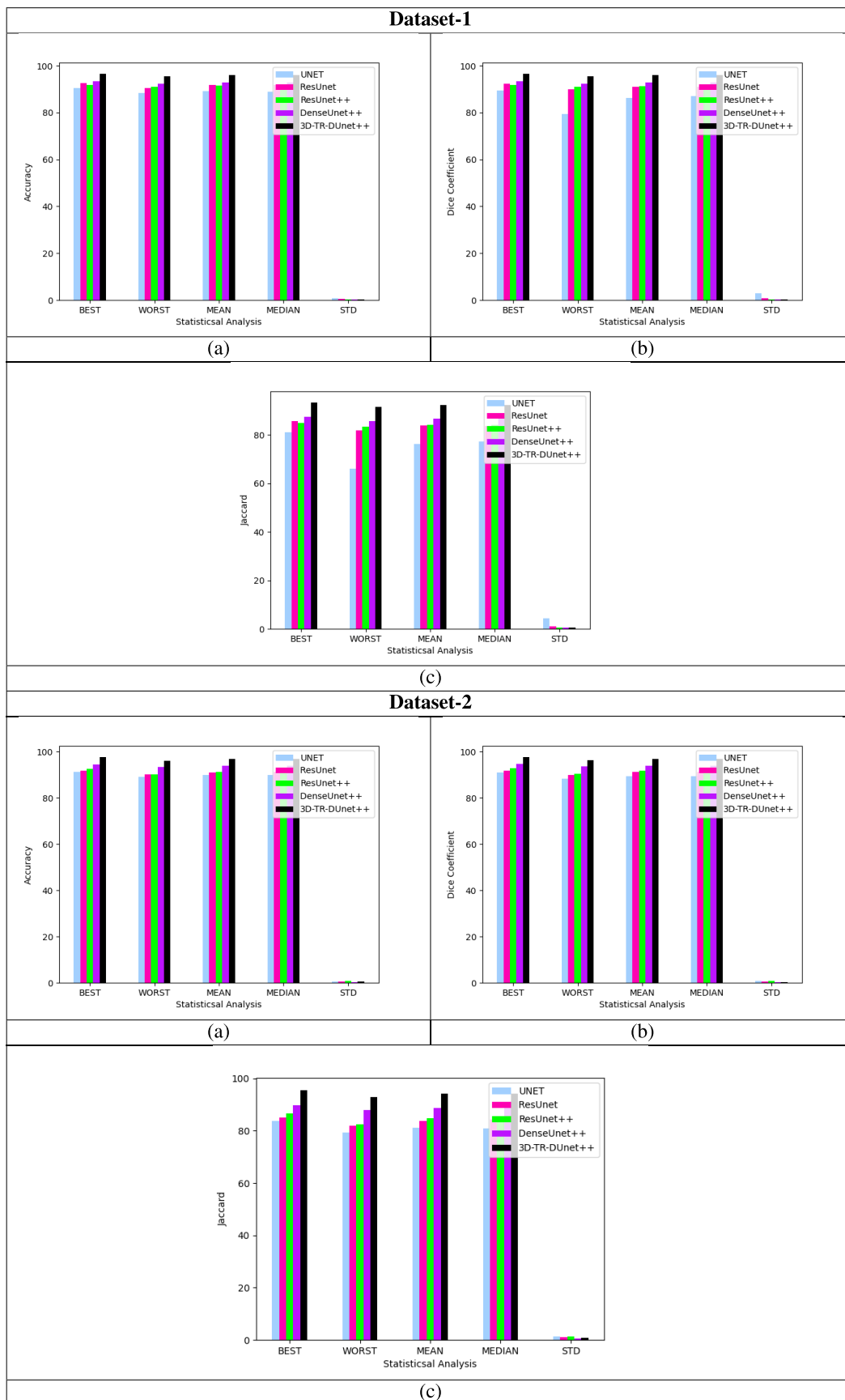


FIGURE 9. Segmentation performance on the designed framework.

TABLE 3. Developed 3D-TR-DUnet++-based segmented images results.

Image Description	Original Image	Ground Truth image	UNET [36]	ResUnet [37]	ResUnet++ [38]	DenseUnet++ [41]	3D-TR-DUnet++
Periapical X-rays Dataset							
“Image 1”							
“Image 2”							
“Image 3”							
“Image 4”							
“Image 5”							
IDental-panoramic Dataset							
“Image 1”							
“Image 2”							
“Image 3”							
“Image 4”							
“Image 5”							

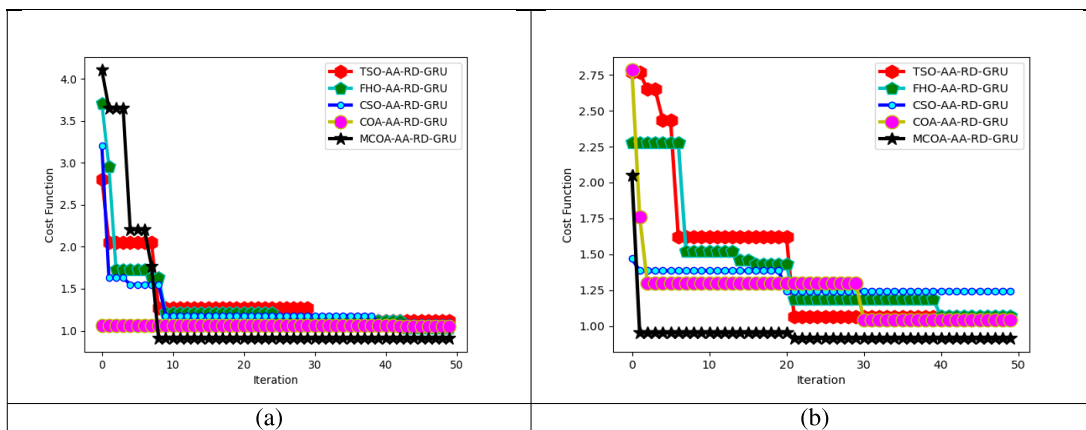


FIGURE 10. ROC analysis on the developed MCOA-AA-RD-GRU-based classification model regarding (a) Dataset-1, and (b) dataset-2.

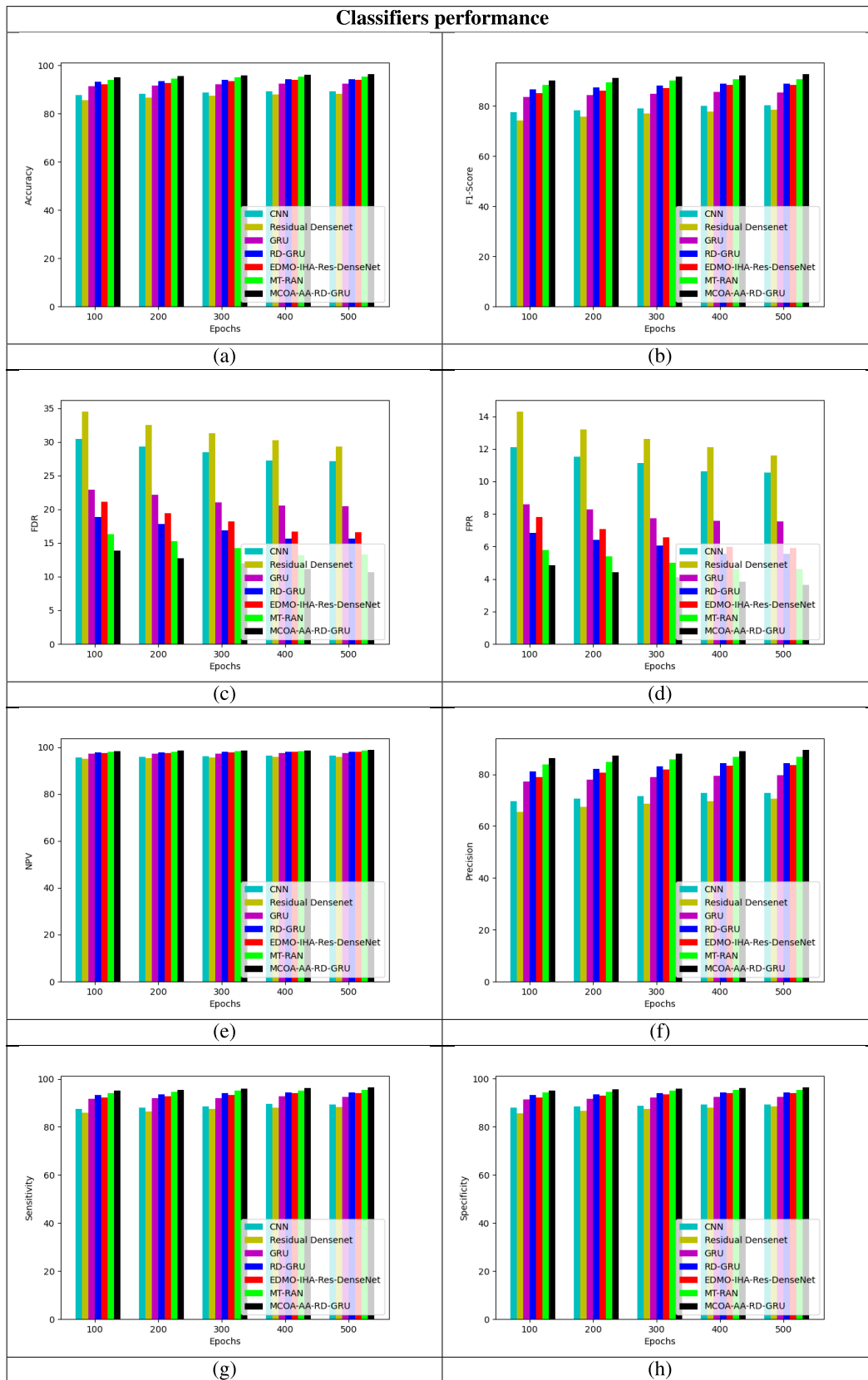


FIGURE 11. Dataset-1-based classification performance evaluation on the recommended model.

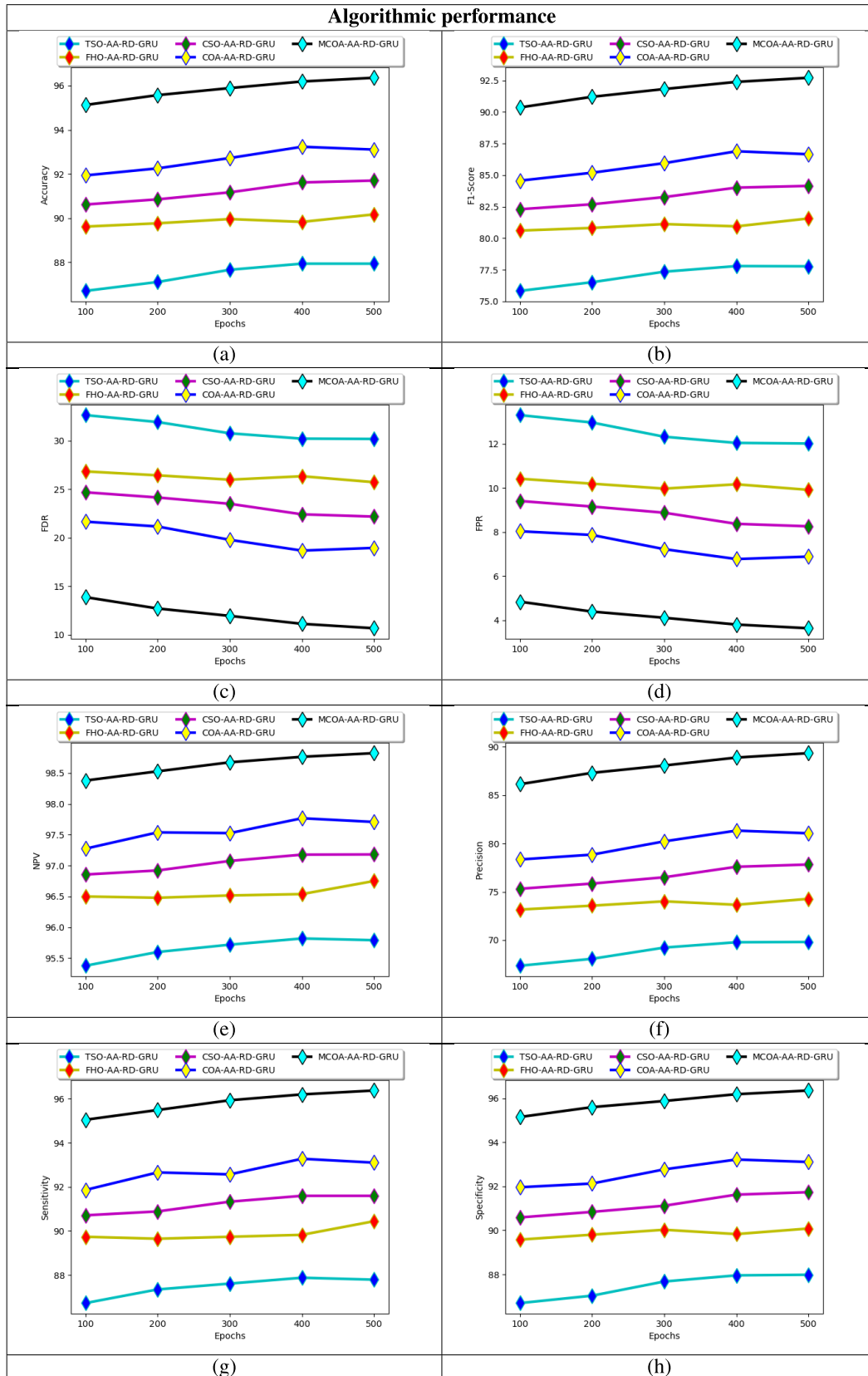


FIGURE 12. Dataset-1-based algorithm performance evaluation on the recommended model.

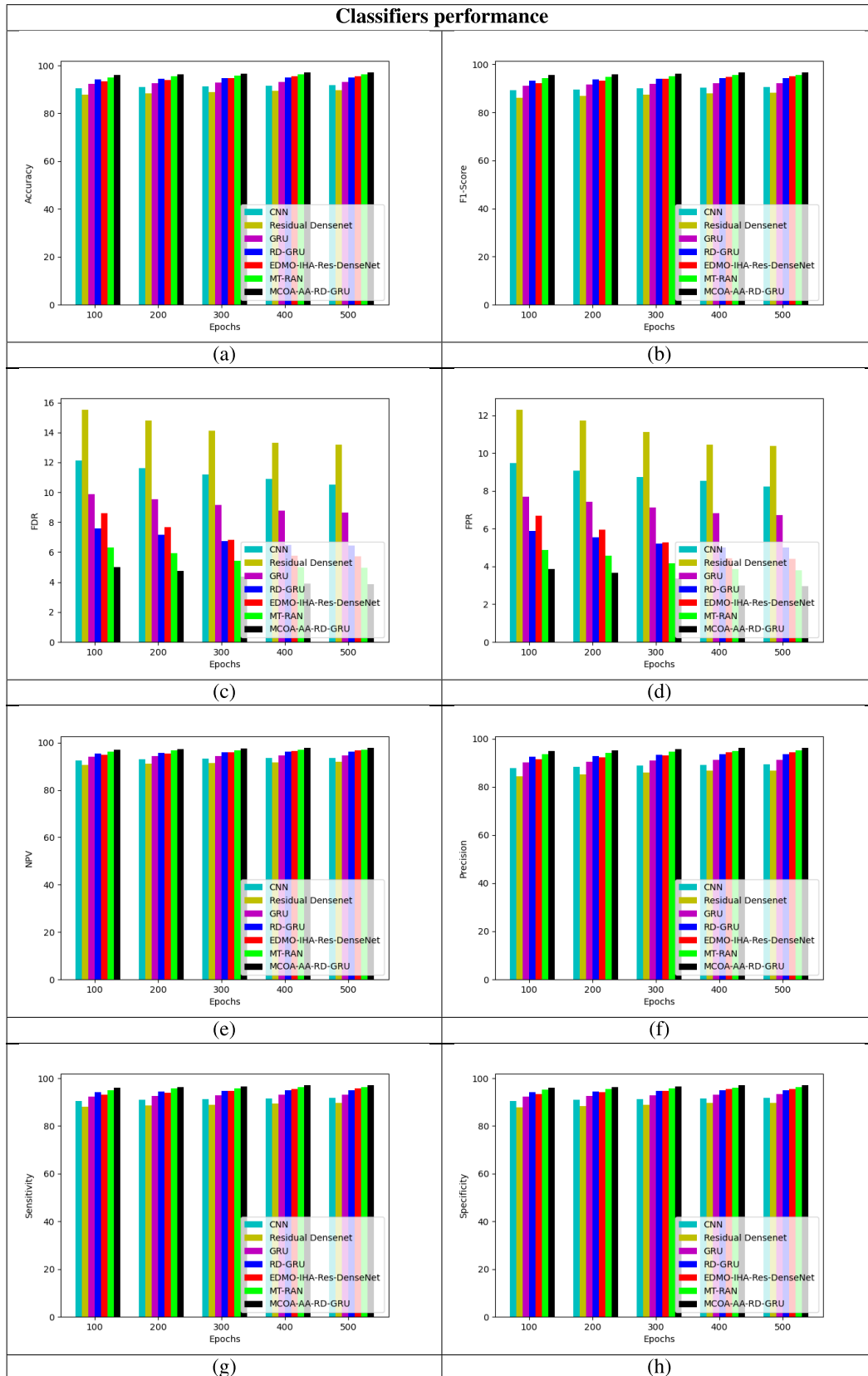


FIGURE 13. Dataset-2-based classification performance evaluation on the recommended model.

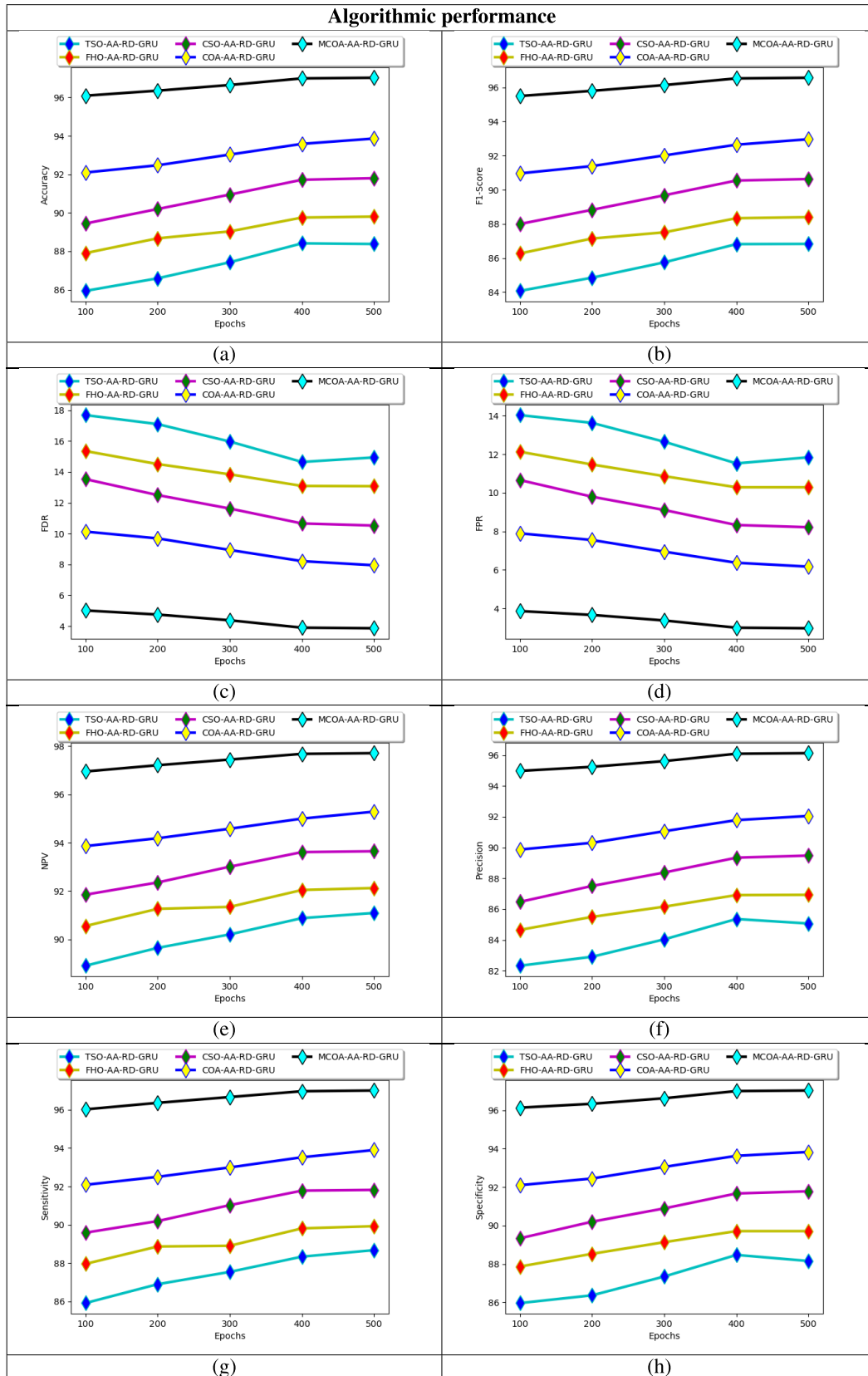


FIGURE 14. Dataset-2-based algorithm performance evaluation on the recommended model.

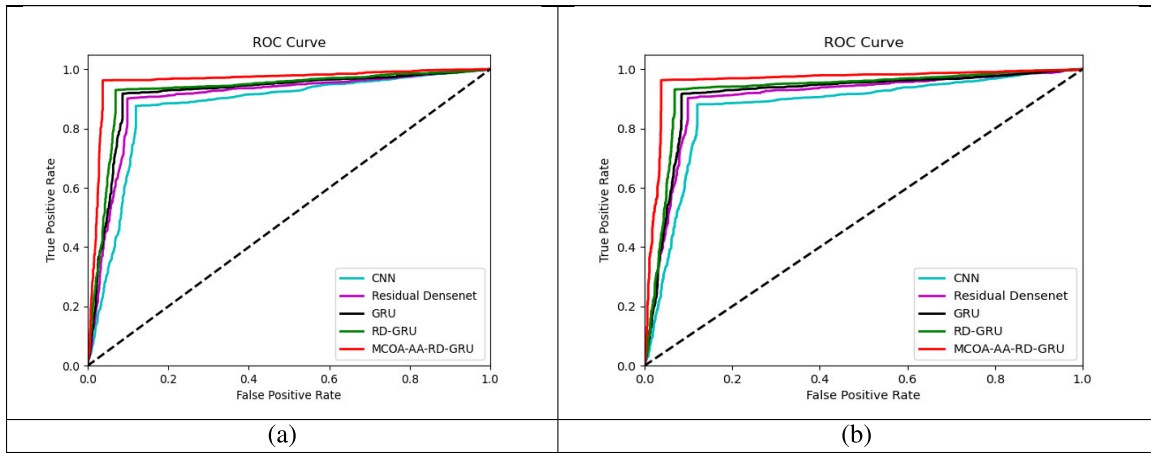


FIGURE 15. ROC Analysis on the developed MCOA-AA-RD-GRU-based classification model regarding (a) Dataset-1, and (b) dataset-2.

TABLE 4. Overall comparison evaluation of the recommended model with existing algorithms.

TERMS	TSO-AA-RD-GRU [33]	FHO-AA-RD-GRU [34]	CSO-AA-RD-GRU [35]	COA-AA-RD-GRU [26]	MCOA-AA-RD-GRU
Dataset-1					
Accuracy	87.936	90.170	91.702	93.106	96.362
Recall	87.788	90.442	91.593	93.097	96.372
Specificity	87.983	90.084	91.737	93.109	96.359
Precision	69.810	74.273	77.820	81.048	89.336
FPR	12.017	9.916	8.263	6.891	3.641
FNR	12.212	9.558	8.407	6.903	3.628
NPV	95.791	96.751	97.181	97.707	98.822
FDR	30.190	25.727	22.180	18.952	10.664
F1-Score	77.773	81.564	84.146	86.656	92.720
MCC	0.705	0.756	0.791	0.824	0.904
Dataset-2					
Accuracy	88.380	89.804	91.800	93.863	97.021
Recall	88.674	89.924	91.818	93.902	97.008
Specificity	88.156	89.712	91.787	93.833	97.032
Precision	85.065	86.928	89.480	92.053	96.134
FPR	11.844	10.288	8.213	6.167	2.968
FNR	11.326	10.076	8.182	6.098	2.992
NPV	91.096	92.128	93.649	95.288	97.707
FDR	14.935	13.072	10.520	7.947	3.866
F1-Score	86.832	88.401	90.634	92.968	96.569
MCC	0.765	0.793	0.834	0.875	0.939

for elective procedures such as an operation, which reduces patient suffering and time to recovery.

G. DATASET-2-BASED CLASSIFICATION PERFORMANCE EVALUATION ON THE RECOMMENDED MODEL

Fig. 13 and 14 illustrate the performance results of the created MCOA-AA-RD-GRU-based classification model compared to current classifiers and optimization methodologies considering dataset 2. The NPV of the proposed MCOA-AA-RD-GRU model is 8.77%, 11.75%, 8.65%, 4.93%, 3.16%, and 2.27% effective than CNN, Residual Densenet, GRU, RD-GRU, PBS-SO-OHFD and IDF-HBA-OEC at 200th epoch. The recommended MCOA-AA-RD-GRU-based classification model offered a precision is 16.54% more

than TSO-AA-RD-GRU, 13.96% superior to FHO-AA-RD-GRU, 11.5% enhanced than CSO-AA-RD-GRU, and 7.22% increased than COA-AA-RD-GRU at 300th epoch. The result proved the proposed MCOA-AA-RD-GRU framework provides vital information for the study and creation of unique ways for treatment.

H. ROC ANALYSIS ON THE DEVELOPED MODEL

Fig. 15 shows the ROC analysis of the developed model. The developed model provided the true positive value is 2.08%, 4.255%, 8.88%, and 13.95% more effective than CNN, Residual DenseNet, GRU, and RD-GRU when the false positive is at 0.4. The result confirmed that the

TABLE 5. Overall comparison evaluation on the recommended model with existing classifiers.

TERMS	CNN [40]	Residual DenseNet [32]	GRU [31]	RD-GRU [39]	PBS-SO-OHFD [42]	IDF-HBA-OEC [43]	MCOA-AA-RD-GRU
Dataset-1							
Accuracy	89.426	88.362	92.447	94.404	94.064	95.383	96.362
Recall	89.381	88.230	92.389	94.248	93.982	95.398	96.372
Specificity	89.440	88.403	92.465	94.454	94.090	95.378	96.359
Precision	72.819	70.659	79.513	84.323	83.425	86.726	89.336
FPR	10.560	11.597	7.535	5.546	5.910	4.622	3.641
FNR	10.619	11.770	7.611	5.752	6.018	4.602	3.628
NPV	96.378	95.956	97.461	98.109	98.016	98.496	98.822
FDR	27.181	29.341	20.487	15.677	16.575	13.274	10.664
F1-Score	80.254	78.473	85.469	89.010	88.390	90.855	92.720
MCC	0.739	0.714	0.808	0.855	84.691	0.880	0.904
Dataset-2							
Accuracy	91.751	89.673	93.224	95.008	95.630	96.187	97.021
Recall	91.705	89.735	93.144	95.000	95.682	96.174	97.008
Specificity	91.787	89.625	93.285	95.014	95.591	96.196	97.032
Precision	89.468	86.808	91.345	93.547	94.289	95.058	96.134
FPR	8.213	10.375	6.715	4.986	4.409	3.804	2.968
FNR	8.295	10.265	6.856	5.000	4.318	3.826	2.992
NPV	93.566	91.985	94.705	96.150	96.677	97.063	97.707
FDR	10.532	13.192	8.655	6.453	5.711	4.942	3.866
F1-Score	90.572	88.247	92.236	94.268	94.980	95.613	96.569
MCC	0.833	0.791	0.862	0.899	91.119	0.922	0.939

TABLE 6. Statistical analysis on the recommended model.

Terms	TSO-AA-RD-GRU [33]	FHO-AA-RD-GRU [34]	CSO-AA-RD-GRU [35]	COA-AA-RD-GRU [26]	MCOA-AA-RD-GRU
Dataset-1					
Worst	2.808	3.706	3.202	1.065	4.103
Best	1.118	1.035	1.099	1.050	0.906
Mean	1.350	1.308	1.267	1.063	1.230
Median	1.270	1.167	1.181	1.065	0.906
Standard deviation	0.368	0.467	0.319	0.005	0.818
Dataset-2					
Worst	2.767	2.281	1.468	2.783	2.050
Best	1.064	1.068	1.242	1.040	0.912
Mean	1.418	1.398	1.301	1.233	0.951
Median	1.064	1.187	1.242	1.297	0.914
Standard deviation	0.510	0.388	0.073	0.266	0.158

developed model outscored the performance of other models by providing the best analysis.

I. OVERALL COMPARISON EVALUATION OF THE RECOMMENDED MODEL WITH EXISTING ALGORITHMS

Table 4 shows the comparison analysis of the developed MCOA-AA-RD-GRU-based classification model compared to current optimization approaches considering dataset-1 and dataset-2. The recommended MCOA-AA-RD-GRU-based classification model offered the F1-Score is 19.21% more than TSO-AA-RD-GRU, 13.67% superior to FHO-AA-RD-GRU, 10.18% enhanced than CSO-AA-RD-GRU, and 6.99% increased than COA-AA-RD-GRU in database-1. The recommended MCOA-AA-RD-GRU model given the Recall is 9.39% more than TSO-AA-RD-GRU, 7.87% superior to FHO-AA-RD-GRU, 5.65% enhanced than CSO-AA-RD-GRU, and 3.3% increased than COA-AA-RD-GRU in database-2. The result proved the proposed

MCOA-AA-RD-GRU framework helps patients make more educated decisions by giving them more knowledge regarding their tumour type, outcome, and available treatments.

J. OVERALL COMPARISON EVALUATION ON THE RECOMMENDED MODEL WITH CLASSIFIERS

Table 5 demonstrates the performance results of the created MCOA-AA-RD-GRU-based classification model compared to current classifiers and optimization methodologies considering dataset 1. The proposed MCOA-AA-RD-GRU model given the specificity is 7.73% more than CNN, 8.99% superior to Residual Densenet, 4.21% enhanced than GRU, 2.02% increased than RD-GRU, 2.41% improved than PBS-SO-OHFD and 1.02% effective than IDF-HBA-OEC in dataset-1. The FPR of the proposed MCOA-AA-RD-GRU model is 63.86% more effective than CNN, 71.39% better than Residual Densenet, 55.8% superior to GRU, 40.47% better than RD-GRU, 32.68% improved than PBS-SO-OHFD

and 21.97% effective than IDF-HBA-OEC in dataset-2. The result confirmed the suggested MCOA-AA-RD-GRU system guarantees accuracy and uniformity in the evaluation of tumours, lowering variation and enhancing overall control of quality in the testing process.

K. STATISTICAL ANALYSIS ON THE RECOMMENDED MODEL

Table 6 shows the statistical analysis of the developed MCOA-AA-RD-GRU-based classification model regarding dataset-1 and Dataset 2. The recommended MCOA-AA-RD-GRU-based classification model offered the best value is 14.28% more than TSO-AA-RD-GRU, 14.6% superior to FHO-AA-RD-GRU, 26.57% enhanced than CSO-AA-RD-GRU, and 12.3% increased than COA-AA-RD-GRU in database-2. The result proved the proposed MCOA-AA-RD-GRU framework inspires patients by helping them with their cancer kind, allowing individuals to actively engage in the therapeutic process.

X. CONCLUSION AND FUTURE DIRECTION

The developed kidney tumour segmentation and classification model based on a deep learning strategy helped in the initial identification of kidney tumours, allowing for swift action and a greater likelihood of survival. Initially, the input CT images were collected from regular sources. The images are subsequently inputted into the developed 3D-TR-DUnet++ system for segmentation. The segmented images then proceeded to the classification phase. To classify kidney tumours, an AA-RD-GRU-based classification model was developed. The parameters in the developed AA-RD-GRU system like hidden neurons, epochs, and step per epoch, were optimized using the suggested MCOA to enhance accuracy. The performance was validated with the conventional model and showed its effectiveness than others. During comparison, the precision of the proposed MCOA-AA-RD-GRU-based classification model is 7.45% more than CNN, 10.74% superior to Residual Densenet, 5.24% enhanced than GRU, 2.76% increased than RD-GRU, 1.95% improved than PBS-SO-OHFD, and 1.13% effective than IDF-HBA-OEC. The standard deviation of the recommended MCOA-AA-RD-GRU-based classification model is 55% more than TSO-AA-RD-GRU, 75.1% superior to FHO-AA-RD-GRU, 61% enhanced than CSO-AA-RD-GRU, and 99.38% increased than COA-AA-RD-GRU. The result confirmed the suggested MCOA-AA-RD-GRU system helps create efficient follow-up plans depending on the features of the tumour, guaranteeing prompt recognition of migration or recurring. The implemented kidney tumour classification system offered highly accurate outcomes. Moreover, it minimizes the computational burdens. However, while processing large-scale datasets, the quality of the outcome is minimized. Hence, in future work, more effective techniques will be integrated into the suggested work to improve the quality of the outcome. Moreover, the designed system has not classified the cancer subtypes. Therefore,

in future work, the designed kidney tumour classification system will be improved for classifying the tumour subtypes to offer valuable data for further experiments. This will also support medical experts in making better treatment decisions.

ACKNOWLEDGMENT

The research work has been carried out with the joint collaboration of the authors. The authors would like to thank the medical experts and representatives. The data has been arranged as per the standards of medical protocols.

REFERENCES

- [1] L. Kang, Z. Zhou, J. Huang, and W. Han, "Renal tumors segmentation in abdomen CT images using 3D-CNN and ConvLSTM," *Biomed. Signal Process. Control*, vol. 72, Feb. 2022, Art. no. 103334.
- [2] L. Corbat, J. Henriet, Y. Chaussy, and J.-C. Lapayre, "Fusion of multiple segmentations of medical images using OV2ASSION and deep learning methods: Application to CT-scans for tumoral kidney," *Comput. Biol. Med.*, vol. 124, Sep. 2020, Art. no. 103928.
- [3] L. B. da Cruz, D. A. D. Júnior, J. O. B. Diniz, A. C. Silva, J. D. S. de Almeida, A. C. de Paiva, and M. Gattass, "Kidney tumor segmentation from computed tomography images using DeepLabv3+ 2.5D model," *Expert Syst. Appl.*, vol. 192, Apr. 2022, Art. no. 116270.
- [4] W. Zhao, D. Jiang, J. P. Queralt, and T. Westerlund, "MSS U-net: 3D segmentation of kidneys and tumors from CT images with a multi-scale supervised U-net," *Informat. Med. Unlocked*, vol. 19, 2020, Art. no. 100357.
- [5] Z. Gong and L. Kan, "Segmentation and classification of renal tumors based on convolutional neural network," *J. Radiat. Res. Appl. Sci.*, vol. 14, no. 1, pp. 412–422, Dec. 2021.
- [6] P. Xuan, H. Cui, H. Zhang, T. Zhang, L. Wang, T. Nakaguchi, and H. B. L. Duh, "Dynamic graph convolutional autoencoder with node-attribute-wise attention for kidney and tumor segmentation from CT volumes," *Knowl.-Based Syst.*, vol. 236, Jan. 2022, Art. no. 107360.
- [7] D. Liu, J. Shao, H. Liu, and W. Cheng, "Design on early warning system for renal cancer recurrence based on CNN-based Internet of Things," *IEEE Access*, vol. 10, pp. 34835–34845, 2022.
- [8] D. A. Saleeb, R. M. Helmy, N. F. F. Areeed, M. Marey, K. M. Almustafa, and A. S. Elkorany, "Detection of kidney cancer using circularly polarized patch antenna array," *IEEE Access*, vol. 10, pp. 78102–78113, 2022.
- [9] E. Skounakis, K. Banitsas, A. Badii, S. Tzoulakis, E. Maravelakis, and A. Konstantaras, "ATD: A multiplatform for semiautomatic 3-D detection of kidneys and their pathology in real time," *IEEE Trans. Hum.-Mach. Syst.*, vol. 44, no. 1, pp. 146–153, Feb. 2014.
- [10] M. N. Islam, M. Hasan, M. K. Hossain, M. G. R. Alam, M. Z. Uddin, and A. Soylu, "Vision transformer and explainable transfer learning models for auto detection of kidney cyst, stone and tumor from CT-radiography," *Sci. Rep.*, vol. 12, no. 1, pp. 1–14, Jul. 2022.
- [11] Z. Lin, Y. Cui, J. Liu, Z. Sun, S. Ma, X. Zhang, and X. Wang, "Automated segmentation of kidney and renal mass and automated detection of renal mass in CT urography using 3D U-Net-based deep convolutional neural network," *Eur. Radiol.*, vol. 31, no. 7, pp. 5021–5031, Jul. 2021.
- [12] C. M. Salgado, R. Alaggio, A. Ciolfi, A. Zin, F. Diomedei Camassei, L. Pedace, G. M. Milano, A. Serra, A. Di Giannatale, A. Mastronuzzi, A. Gianatti, G. Bisogno, A. Ferrari, M. Tartaglia, M. Reyes-Múgica, F. Locatelli, and E. Miele, "Pediatric BCOR-altered tumors from soft tissue/kidney display specific DNA methylation profiles," *Modern Pathol.*, vol. 36, no. 2, Feb. 2023, Art. no. 100039.
- [13] R. Li, J. R. Ferdinand, K. W. Loudon, G. S. Bowyer, S. Laidlaw, F. Muyas, L. Mamanova, J. B. Neves, L. Bolt, and E. S. Fasouli, "Mapping single-cell transcriptomes in the intra-tumoral and associated territories of kidney cancer," *Cancer Cell*, vol. 40, no. 12, pp. 1583–1599, Dec. 2022.
- [14] A. Calì, L. Cheng, G. Martignoni, S. Zhang, M. Brunelli, and J. N. Eble, "Mixed epithelial and stromal tumours of the kidney with malignant transformation: A clinicopathological study of four cases," *Pathology*, vol. 54, no. 6, pp. 707–720, Oct. 2022.
- [15] J. Causey, J. Stubblefield, J. Qualls, J. Fowler, L. Cai, K. Walker, Y. Guan, and X. Huang, "An ensemble of U-Net models for kidney tumor segmentation with CT images," *IEEE/ACM Trans. Comput. Biol. Bioinf.*, vol. 19, no. 3, pp. 1387–1392, May 2022.

- [16] M. A. Hussain, G. Hamarneh, and R. Garbi, "Cascaded regression neural nets for kidney localization and segmentation-free volume estimation," *IEEE Trans. Med. Imag.*, vol. 40, no. 6, pp. 1555–1567, Jun. 2021.
- [17] C.-H. Hsiao, T.-L. Sun, P.-C. Lin, T.-Y. Peng, Y.-H. Chen, C.-Y. Cheng, F.-J. Yang, S.-Y. Yang, C.-H. Wu, F. Y.-S. Lin, and Y. Huang, "A deep learning-based precision volume calculation approach for kidney and tumor segmentation on computed tomography images," *Comput. Methods Programs Biomed.*, vol. 221, Jun. 2022, Art. no. 106861.
- [18] S. Pavarut, W. Preedanan, I. Kumazawa, K. Suzuki, M. Kobayashi, H. Tanaka, J. Ishioka, Y. Matsuoka, and Y. Fuji, "Improving kidney tumor classification with multi-modal medical images recovered partially by conditional CycleGAN," *IEEE Access*, vol. 11, pp. 146250–146261, 2023.
- [19] Q. Yu, Y. Shi, J. Sun, Y. Gao, J. Zhu, and Y. Dai, "Crossbar-net: A novel convolutional neural network for kidney tumor segmentation in CT images," *IEEE Trans. Image Process.*, vol. 28, no. 8, pp. 4060–4074, Aug. 2019.
- [20] C.-H. Hsiao, P.-C. Lin, L.-A. Chung, F. Y.-S. Lin, F.-J. Yang, S.-Y. Yang, C.-H. Wu, Y. Huang, and T.-L. Sun, "A deep learning-based precision and automatic kidney segmentation system using efficient feature pyramid networks in computed tomography images," *Comput. Methods Programs Biomed.*, vol. 221, Jun. 2022, Art. no. 106854.
- [21] Y. Ruan, D. Li, H. Marshall, T. Miao, T. Cossetto, I. Chan, O. Daher, F. Accorsi, A. Goela, and S. Li, "MB-FSGAN: Joint segmentation and quantification of kidney tumor on CT by the multi-branch feature sharing generative adversarial network," *Med. Image Anal.*, vol. 64, Aug. 2020, Art. no. 101721.
- [22] P. Russo, K. A. Blum, S. Weng, N. Graafland, and A. Bex, "Outcomes for atypical tumor recurrences following minimally invasive kidney cancer operations," *Eur. Urology Open Sci.*, vol. 40, pp. 125–132, Jun. 2022.
- [23] R. Jikuya, K. Murakami, A. Nishiyama, I. Kato, M. Furuya, J. Nakabayashi, J. A. Ramilowski, H. Hamanoue, K. Maejima, and M. Fujita, "Single-cell transcriptomes underscore genetically distinct tumor characteristics and microenvironment for hereditary kidney cancers," *iScience*, vol. 25, no. 6, Jun. 2022, Art. no. 104463.
- [24] J. Zheng, Y. Mei, G. Zhai, N. Zhao, D. Jia, and Y. Fan, "Downregulation of RUNX3 has a poor prognosis and promotes tumor progress in kidney cancer," *Urologic Oncol., Seminars Original Investigations*, vol. 38, no. 9, pp. 740.e11–740.e20, Sep. 2020.
- [25] H. Jia, H. Rao, C. Wen, and S. Mirjalili, "Crayfish optimization algorithm," *Artif. Intell. Rev.*, vol. 56, no. S2, pp. 1919–1979, Nov. 2023.
- [26] X. Xu, M. An, J. Zhang, W. Liu, and L. Lu, "A high-precision classification method of mammary cancer based on improved DenseNet driven by an attention mechanism," *Comput. Math. Methods Med.*, vol. 2022, pp. 1–14, May 2022.
- [27] E. Bousias Alexakis and C. Armenakis, "Evaluation of UNet and UNet++ architectures in high resolution image change detection applications," *Int. Arch. Photogramm., Remote Sens. Spatial Inf. Sci.*, vol. 43, pp. 1507–1514, Aug. 2020.
- [28] C. Che, P. Zhang, M. Zhu, Y. Qu, and B. Jin, "Constrained transformer network for ECG signal processing and arrhythmia classification," *BMC Med. Informat. Decis. Making*, vol. 21, no. 1, p. 184, Dec. 2021.
- [29] D. Sarwinda, R. H. Paradisa, A. Bustamam, and P. Anggia, "Deep learning in image classification using residual network (ResNet) variants for detection of colorectal cancer," *Proc. Comput. Sci.*, vol. 179, pp. 423–431, 2021.
- [30] X. He and Y. Chen, "Optimized input for CNN-based hyperspectral image classification using spatial transformer network," *IEEE Geosci. Remote Sens. Lett.*, vol. 16, no. 12, pp. 1884–1888, Dec. 2019.
- [31] Y. Zhang, Y. Tian, Y. Kong, B. Zhong, and Y. Fu, "Residual dense network for image super-resolution," in *Proc. IEEE/CVF Conf. Comput. Vis. Pattern Recognit.*, Jun. 2018, pp. 2472–2481.
- [32] L. Xiong, L. Zhang, X. Huang, X. Yang, W. Huang, H. Zeng, and H. Tang, "DCAST: A spatiotemporal model with DenseNet and GRU based on attention mechanism," *Math. Problems Eng.*, vol. 2021, pp. 1–12, Feb. 2021.
- [33] X. Liu, B. Zhang, X. Li, S. Liu, C. Yue, and S. Y. Liang, "An approach for tool wear prediction using customized DenseNet and GRU integrated model based on multi-sensor feature fusion," *J. Intell. Manuf.*, vol. 34, no. 2, pp. 885–902, Feb. 2023.
- [34] Y. Wang, L. Gu, T. Jiang, and F. Gao, "MDE-UNet: A multitask deformable UNet combined enhancement network for farmland boundary segmentation," *IEEE Geosci. Remote Sens. Lett.*, vol. 20, pp. 1–5, 2023.
- [35] R. Li, S. Zheng, C. Duan, J. Su, and C. Zhang, "Multistage attention ResU-net for semantic segmentation of fine-resolution remote sensing images," *IEEE Geosci. Remote Sens. Lett.*, vol. 19, pp. 1–5, 2022.
- [36] D. Jha, P. H. Smedsrud, D. Johansen, T. de Lange, H. D. Johansen, P. Halvorsen, and M. A. Riegler, "A comprehensive study on colorectal polyp segmentation with ResUNet++, conditional random field and test-time augmentation," *IEEE J. Biomed. Health Informat.*, vol. 25, no. 6, pp. 2029–2040, Jun. 2021.
- [37] X. Li, H. Chen, X. Qi, Q. Dou, C.-W. Fu, and P.-A. Heng, "H-DenseUNet: Hybrid densely connected UNet for liver and tumor segmentation from CT volumes," *IEEE Trans. Med. Imag.*, vol. 37, no. 12, pp. 2663–2674, Dec. 2018.
- [38] L. Xie, T. Han, H. Zhou, Z.-R. Zhang, B. Han, and A. Tang, "Tuna swarm optimization: A novel swarm-based metaheuristic algorithm for global optimization," *Comput. Intell. Neurosci.*, vol. 2021, pp. 1–22, Oct. 2021.
- [39] M. Azizi, S. Talatahari, and A. H. Gandomi, "Fire hawk optimizer: A novel metaheuristic algorithm," *Artif. Intell. Rev.*, vol. 56, no. 1, pp. 287–363, Jan. 2023.
- [40] M. H. Qais, H. M. Hasanien, R. A. Turkey, S. Alghuwainem, M. Tostado-Véliz, and F. Jurado, "Circle search algorithm: A geometry-based metaheuristic optimization algorithm," *Mathematics*, vol. 10, no. 10, p. 1626, May 2022.



VINITKUMAR VASANTBHAI PATEL received the B.E. degree in electronics and communication engineering from North Maharashtra University, Jalgaon, in 2007, and the M.E. degree in communication engineering from Dr. Babasaheb Ambedkar Marathwada University, Aurangabad, in 2014. He is currently pursuing the Ph.D. degree with the Department of Electronics and Communication Engineering, Parul Institute of Engineering and Technology, FET, Parul University, Vadodara, India. He is a Research Scholar with the Department of Electronics and Communication Engineering, Parul Institute of Engineering and Technology, FET, Parul University. His research interests include image processing, deep learning, and the Internet of Things.



ARVIND R. YADAV received the B.E. degree in electronics and communication engineering from GEC, Modasa, in 1999, the M.E. degree in industrial electronics from MSU, Baroda, in 2001, and the Ph.D. degree in image processing from the Electrical Engineering Department, IIT Roorkee, in 2016. He is currently an Associate Professor with the Department of Electronics and Instrumentation Engineering, Institute of Technology, Nirma University, Ahmedabad. He has published several research papers in peer-reviewed journals and conferences. He has completed an international research grant awarded by the Royal Academy of Engineering, U.K. His research interests include signal, image, and video processing (feature extraction), especially medical signal and image and microscopic images of wood species. He is also actively working in the area of object recognition and classification with the help of machine learning and deep learning techniques. He has been a reviewer of several reputed journals and conferences.



PRATEEK JAIN (Member, IEEE) received the B.E. degree in electronics engineering from Jiwaji University, India, in 2010, the master's degree from ITM University, Gwalior, and the Ph.D. degree from MNIT Jaipur, Rajasthan, in 2020. He is currently an Assistant Professor with the Electronics and Instrumentation Engineering Department, Nirma University, Ahmedabad, India. He has published several research papers in peer-reviewed journals and conferences. He is also a reviewer of reputed journals and conferences. He got three research seed grants at the university level. His research interests include real-time system design for biomedical applications, analog circuits, digital VLSI design, and machine learning for computation. He is a member of IEI and SPIE. He was awarded from MHRD Fellowship.



LINGA REDDY CENKERAMADDI (Senior Member, IEEE) received the master's degree in electrical engineering from the Indian Institute of Technology Delhi (IIT Delhi), New Delhi, India, in 2004, and the Ph.D. degree in electrical engineering from the Norwegian University of Science and Technology (NTNU), Trondheim, Norway, in 2011. He was with Texas Instruments on mixed signal circuit design before joining the Ph.D. program with NTNU. After finishing his Ph.D. degree, he worked on radiation imaging for an atmosphere-space interaction monitor (ASIM mission to the International Space Station) with the University of Bergen, Bergen, Norway, from 2010 to 2012. He is currently a Leader of the Autonomous and Cyber-Physical Systems (ACPS) Research Group and a Professor with the University of Agder, Grimstad, Norway. He is a Principal Investigator and a Co-Principal Investigator of many research grants from the Norwegian Research Council. He is also quite active in medical imaging. His research interests include the Internet of Things (IoT), cyber-physical systems, autonomous systems, robotics and automation involving advanced sensor systems, computer vision, thermal imaging, LiDAR imaging, radar imaging, wireless sensor networks, smart electronic systems, advanced machine learning techniques, and connected autonomous systems, including drones/unmanned aerial vehicles (UAVs), unmanned ground vehicles (UGVs), unmanned underwater systems (UUSs), 5G- (and beyond) enabled autonomous vehicles, and socio-technical systems, such as urban transportation systems, smart agriculture, and smart cities. He has coauthored more than 200 research publications that have been published in prestigious international journals and standard conferences in the above research areas. He is a member of ACM. He is a member of the editorial boards of various international journals and the technical program committees of several IEEE conferences. Several of his master's students received the best master's thesis award in information and communication technology (ICT). He serves as a reviewer for several reputed international conferences and IEEE journals.

• • •